PML mutants resistant to arsenic induced degradation fail to generate the appropriate SUMO and ubiquitin signals required for RNF4 and p97 recruitment.

Ellis G. Jaffray, Michael H. Tatham, Alejandro Rojas-Fernandez, Adel Ibrahim, Graeme Ball and Ronald T. Hay*

Centre for Gene Regulation and Expression, School of Life Sciences, University of Dundee, Dundee, UK

***Corresponding author**

Email: r.t.hay@dundee.ac.uk

ORCID: 0000-0001-7113-9024

ABSTRACT

Arsenic is an effective treatment for Acute Promyelocytic Leukaemia as it induces degradation of the Promyelocytic Leukaemia (PML) – retinoic acid receptor alpha (RARA) oncogenic fusion protein. Some patients relapse with arsenic resistant disease because of missense mutations in PML. To determine the mechanistic basis for arsenic resistance we reconstituted PML-/- cells with YFP fusions of wild type (WT) and two mutant forms of PMLV found in patients refractory to arsenic, A216T and L217F. Both mutants formed PML bodies that were larger, but less numerous than WT and neither responded to arsenic by degradation. Analysis of immunoprecipitated PML bodies indicated that while WT PML experiences increased SUMO1, SUMO2/3 and ubiquitin conjugation, A216T PML is almost completely unresponsive and therefore does not recruit the SUMO targeted ubiquitin E3 ligase RNF4. Compared to WT PML, L217F PML was modified to a similar extent by SUMO2 but not SUMO1 and although it recruited RNF4, it failed to develop the appropriate poly-ubiquitin conjugates required to recruit the segregase p97, which is essential for PML degradation.

INTRODUCTION

Acute Promyelocytic Leukaemia (APL) is caused by a reciprocal chromosomal translocation t(15;17) that fuses the genes encoding the Promyelocytic Leukaemia (PML) protein and the retinoic acid receptor alpha (RARA) (de The, Lavau et al. 1991, Kakizuka, Miller et al. 1991). This generates the PML-RARA oncoprotein that deregulates transcriptional programmes required for the differentiation of haematopoetic progenitor cells. Therefore, differentiation is blocked and promyelocytes accumulate causing leukaemia (Grignani, Ferrucci et al. 1993, Kwok,

42 Zeisig et al. 2006, Martens, Brinkman et al. 2010, Mikesch, Gronemeyer et al. 2010,
43 Tan, Wang et al. 2021). In healthy cells the PML gene is alternatively spliced to
44 generate multiple mRNAs that encode seven protein isoforms (I-VII) that differ in
45 their C-terminal regions.
46
47 PML is a member of the Tripartite Motif (TRIM) family of proteins and is also known
48 as TRIM19. Located in the N-terminal region of PML and present in all PML isoforms
49 and PML-RARA fusions, the highly conserved TRIM is composed of a RING domain,
50 two zinc co-ordinating B-boxes and a coiled-coil that mediates dimerization (Bernardi
51 and Pandolfi 2007). In cells with wild type (WT) PML genes, the protein is associated
52 with non-membranous nuclear structures known as PML nuclear bodies, that also
53 accumulate a variety of other proteins including Small Ubiquitin-like Modifiers
54 (SUMOs), p53, Daxx and SP100. In cells containing a PML-RARA fusion protein,
55 PML and PML-RARA are co-associated in a large number of tiny nuclear speckles
56 (Dyck, Maul et al. 1994, Weis, Rambaud et al. 1994). In the past, treatment options
57 were limited and APL was a disease with a very poor prognosis. However, the
58 majority of patients are now cured by a combination therapy consisting of arsenic
59 trioxide (referred to herein as As) and *all trans* retinoic acid (ATRA) (Wang and Chen
60 2008, Lo-Coco, Avvisati et al. 2013, Mi, Chen et al. 2015). These induce degradation
61 of the PML-RARA oncogene and allows the WT version of RARA to initiate a
62 transcriptional programme that drives the accumulated promyelocytes down a
63 pathway of terminal differentiation that ultimately cures the disease. Arsenic alone
64 induces degradation of both the unfused PML and PML-RARA, identifying PML as
65 the target of As. Treatment with As leads to rapid multisite modification of PML and
66 PML-RARA with SUMO (Muller, Matunis et al. 1998). SUMO modified PML and

PML-RARA then serves to recruit the SUMO Targeted Ubiquitin E3 ligase (STUbL) RING Finger Protein 4 (RNF4) (Perry, Tainer et al. 2008, Geoffroy and Hay 2009). Recruitment of RNF4 to SUMO modified PML and PML-RARA present in PML nuclear bodies is mediated by multiple SUMO Interaction Motifs (SIMs) present in the N-terminal region of the protein. The high local concentration of RNF4 leads to dimerization of the C-terminal RING domains and activation of the ubiquitin E3 ligase activity of the protein (Rojas-Fernandez, Plechanovova et al. 2014). RNF4 mediated ubiquitination of SUMO modified PML and PML-RARA ultimately leads to their proteolytic degradation by the proteasome (Lallemand-Breitenbach, Jeanne et al. 2008, Tatham, Geoffroy et al. 2008). Recently, an additional step required for arsenic induced degradation of PML and PML-RARA has been uncovered that involves the p97/VCP segregase (Jaffray, Tatham et al. 2023). RNF4 mediated ubiquitination of PML leads to recruitment of UFD1-NPLOC4-p97 which extracts ubiquitinated PML and presumably feeds the modified protein to the proteasome where it is proteolytically degraded.

While the majority of APL patients treated with As are cured, a small proportion of these patients relapse and present with arsenic resistant disease. In some cases resistance may be a consequence of metabolic reprogramming linked to expression of additional known oncogenes (Madan, Shyamsunder et al. 2016, Iaccarino, Ottone et al. 2019), but in many patients, arsenic resistance is a result of missense mutations in PML clustered between residues L211 and S220 in B-box 2. These mutations are not only found in the PML-RARA oncogene (Goto, Tomita et al. 2011, Chendamarai, Ganesan et al. 2015, Lou, Ma et al. 2015, Iaccarino, Ottone et al. 2016, Liu, Zhu et al. 2016) but also in the unfused version of PML (Lehmann-Che,

92 Bally et al. 2014, Zhu, Qin et al. 2014, Iaccarino, Ottone et al. 2016). These
93 mutations are undetectable at initial diagnosis, suggesting that cells expressing
94 these mutations are selected for by arsenic treatment (Alfonso, Iaccarino et al. 2019,
95 Balasundaram, Ganesan et al. 2022).
96
97 To establish the mechanistic basis for the arsenic resistance we investigated the
98 properties of two mutations in PML that responded differently to As. While both
99 mutations were resistant to As-induced degradation, the A216T mutant was severely
100 compromised for SUMO modification, failed to recruit RNF4 and as a result was not
101 ubiquitinated. In contrast, like WT PML the L217F mutant was modified by
102 SUMO2/3, recruited RNF4, and was ubiquitinated in response to As. However,
103 SUMO1 modification was compromised and the ubiquitin signal was not sufficient to
104 recruit the p97 segregase that is required to extract PML from nuclear bodies. Thus,
105 while two mutations that are adjacent in the PML B-box both inhibit As-induced PML
106 degradation, mechanistic failure is at different steps of the degradation pathway.
107
108 **RESULTS**
109 **PML mutants A216T and L217F form atypical PML bodies in U2OS cells.**
110 Mutations in PML and PML-RARA that arise in APL patients with arsenic resistant
111 disease are a unique resource as these mutations are selected in vivo to be resistant
112 to arsenic while still retaining the biological functions of PML that contribute to the
113 disease phenotype. The majority of these mutations are located to a 10 amino acid
114 region (L211-S220) in B-box 2 of PML that encompasses, but never includes, the
115 zinc co-ordinating residues C212 and C215 (Fig. 1A). As PML is the direct target of
116 arsenic and mutations from patients with arsenic resistant disease can also be

117 detected in the non-rearranged allele of PML (Lehmann-Che, Bally et al. 2014,
118 Iaccarino, Ottone et al. 2016), we chose to reconstitute U2OS PML-/- cells with wild-
119 type (WT) or mutant versions of PMLV N-terminally fused to YFP (Jaffray, Tatham et
120 al. 2023). In testing a number of PML variants, we found that they fell into two main
121 groups exemplified by the most frequently identified mutations in patients; A216T
122 and L217F. U2OS cells expressing YFP fused forms of WT, A216T and L217F
123 PMLV were isolated by FACS and the derived cell lines analysed by high content
124 microscopy. Images of these cells show that while the total YFP fluorescence signal
125 was similar for WT, A216T and L217F, the average size and number of PML bodies
126 per cell varied (Fig. 1B). Quantitative analysis of thousands of cells showed that the
127 average expression levels, measured by YFP-PML intensity per cell, were similar for
128 all three PML forms (Fig. 1C). However, cells expressing A216T and L217F PMLV
129 had on average approximately half the number of PML bodies per cell (median = 4)
130 compared to WT (median = 8) (Fig. 1C). This was contrasted by both mutants
131 showing larger than WT PML bodies according to their measured cross-sectional
132 area (Fig. 1C). This ~20-25% larger area equates to almost twice the volume when
133 considering a spherical PML body. These results show that A216T and L217F
134 mutations to PML reduce PML body number and increase PML body size in
135 untreated cells.
136
137 **PML mutants A216T and L217F are not degraded in response to arsenic in**
138 **U2OS cells**
139 Arsenic exposure is responsible for dramatic changes to the number, morphology
140 and content of PML bodies (Geoffroy et al., 2010; Jeanne et al., 2010). To determine
141 how these parameters were influenced by mutations in PML, the cells expressing

142 WT, A216T or L217F YFP-PMLV were either untreated or treated with 1μM arsenic
143 and monitored by time-lapse fluorescence microscopy over a 15 hr period. At least 9
144 movies were collected for each condition and an automated, quantitative pipeline
145 (Jaffray, Tatham et al. 2023) was used to follow PML body size, number and total
146 YFP-PMLV fluorescence intensity over time (see Supplementary movies 1-6 for
147 representative time-course data). Representative images from the cells at 0 and 15
148 hr (Fig. 2A) showed the expected reduction in the number and total intensity of
149 nuclear bodies in WT PMLV expressing cells, but not in cells expressing A216T or
150 L217F PMLV (Fig. 2A). Averaged values of these metrics across all time courses
151 indicated that PML body size did not significantly change over time after arsenic
152 treatment for any of the PML forms studied (Fig. 2B). Furthermore, the number of
153 bodies per cell and normalized YFP-PML intensity was reduced during arsenic
154 exposure for WT PML but not for either mutant (Fig. 2B). More specifically, after 15
155 hr As there was a >4 fold reduction in the number of PML bodies per cell and >3 fold
156 reduction in YFP-PMLV intensity for the WT PMLV, while little or no change was
157 observed for A216T and L217F mutants (Fig. 2C). Western-blot analysis of extracts
158 gathered from cells exposed to arsenic over a 24 hr time-course showed that as
159 expected, WT PML rapidly shifts to a higher molecular weight species and is
160 completely degraded by 24 hr (Fig. 2D). In contrast, A216T PML does not appear to
161 shift to a higher molecular weight form and its levels do not change over the 24 hr
162 period. Unlike A216T, L217F PML does shift to higher molecular weight species, but
163 it is not degraded in response to arsenic after 24 hr (Fig. 2D).
164
165 **In response to arsenic, WT and L217F PML recruit RNF4 but the A216T mutant**
166 **does not**

167 Although A216T does not appear to respond to arsenic by altered post-translational
168 modification, both the WT and L217F forms display reduced electrophoretic mobility
169 upon exposure of cells to arsenic (Fig. 2D). To better understand the nature of the
170 modification status of all PML variants, nuclear bodies were purified from WT, A216T
171 and L217F YFP-PMLV expressing cells (Jaffray, Tatham et al. 2023) both before and
172 after treatment with 1μM As for 2h and analysed by Western blot for PML, SUMO1
173 or SUMO2/3. Consistent with the analysis of PML from whole cell extracts (Fig. 2D),
174 purified YFP-PMLV WT and L217F shifted to higher molecular weight species in
175 response to arsenic treatment for 2 hrs, whereas this response was almost
176 completely blunted for A216T (Fig. 3A). SUMO1 modification of all three PML forms
177 in untreated cells appears to be similar, but in response to arsenic, WT YFP-PMLV
178 undergoes a much greater increase in SUMO1 modification than either A216T or
179 L217F mutants. As with SUMO1, in untreated cells conjugation of all three PML
180 forms to SUMO2/3 is broadly comparable (Fig. 3A). However, there are some
181 notable differences in the SUMO2/3 response to arsenic in comparison with SUMO1.
182 Firstly, the scale of the As-induced increase in SUMO2/3 conjugation to WT-PML is
183 not as large as the relative increase in SUMO1. Secondly, both mutants show a
184 SUMO2/3 conjugation response to As treatment, albeit weakest for the A216T
185 mutant (Fig. 3A).
186 Enhanced SUMO modification of PML is responsible for the recruitment of the
187 STUbL RNF4 that mediates PML ubiquitination prior to degradation by the
188 proteasome. To study RNF4 recruitment in response to arsenic, nuclear bodies from
189 WT, A216T and L217F YFP-PMLV expressing cells were again purified and the
190 associated RNF4 determined by Western blotting (Fig. 3B). RNF4 was not stably
191 associated with nuclear bodies in the absence of arsenic, but was detected in

192 purifications containing WT and L217F YFP-PMLV forms after arsenic treatment
193 (Fig. 3B). By this method RNF4 was not detectable in A216T YFP-PMLV
194 purifications in response to arsenic (Fig. 3B). The YFP-PMLV purifications were then
195 analysed for ubiquitin modification by Western blotting with an antibody that detects
196 ubiquitin chains. This revealed that WT YFP-PMLV was extensively ubiquitinated in
197 response to arsenic and, consistent with the failure to recruit RNF4, increase in the
198 ubiquitination of A216T YFP-PMLV was not detected (Fig. 3B). Interestingly,
199 although L217F YFP-PMLV recruited RNF4, the increase in ubiquitin chains was not
200 apparently as great as for the WT protein, and the modified species had a lower
201 molecular weight (Fig. 3B).
202
203 The arsenic-induced recruitment of SUMO1, SUMO2/3 and RNF4 to PML bodies
204 was also analysed by fluorescence microscopy for the three different cell lines. This
205 confirmed that colocalization of SUMO1, SUMO2/3 and RNF4 with PML was
206 increased for the WT protein in response to arsenic (Supplementary Figs. 1-3).
207 Consistent with the Western blot data (Fig. 3A+B), the A216T PML mutant showed
208 little response to arsenic in terms of recruitment of SUMO1, SUMO2/3 or RNF4. The
209 L217F PML variant showed lower than WT recruitment of SUMO1 and SUMO2/3 in
210 response to arsenic (Supplementary Fig. 1&2), although RNF4 levels appeared
211 similar (Supplementary Fig. 3). In this experiment, RNF4 appears to colocalise with
212 PML nuclear bodies prior to arsenic treatment, but this increases in response to
213 arsenic for both WT and L217F and less so for A216T (Supplementary Fig. 3). Thus,
214 both Western blotting and fluorescence microscopy indicate that the inability of
215 A216T PML to be degraded is the consequence of insufficient SUMO conjugation
216 which fails to recruit RNF4, and therefore is not ubiquitinated. This was not the case

217 for L217F which could recruit RNF4 and induce ubiquitination, but was still resistant
218 to degradation.
219
220 **In response to arsenic L217F PML fails to recruit the p97 segregase**
221 Recently we determined that the p97 segregase was required to extract ubiquitinated
222 PML from nuclear bodies prior to degradation by the proteasome (Jaffray, Tatham et
223 al. 2023). To determine if the mutants were compromised for p97 extraction we
224 analysed WT, A216T and L217F YFP-PMLV expressing cells by fluorescence
225 microscopy 0, 2, 4 and 6 hr after arsenic treatment. p97 recruitment was determined
226 by evaluating the extent of co-localisation between antibody stained p97 and PML
227 marked by YFP fluorescence. As p97 is a highly abundant protein we employed a
228 pre-extraction procedure to release the bulk of the soluble p97 from the cells before
229 fixation. In WT YFP-PMLV untreated cells p97 was associated with only a small
230 proportion of PML bodies, whereas after 6 hr arsenic treatment a larger fraction of
231 PML bodies had associated p97 (Supplementary Fig. 4). In cells expressing A216T
232 and L217F YFP-PMLV, arsenic treatment did not appear to increase the association
233 of p97 with PML bodies (Fig. 4A, Supplementary Fig. 4). To quantify this, the
234 percentage of PML bodies co-localised with p97 in WT, A216T and L217F YFP-
235 PMLV expressing cells was determined at 0, 2, 4 and 6 hr after arsenic treatment
236 (Fig. 4B). In untreated WT YFP-PMLV expressing cells about 20% of PML bodies
237 were associated with p97, which increased to over 60% at 2, 4 and 6 hr after arsenic
238 treatment. In untreated cells expressing A216T and L217F YFP-PMLV, p97
239 association was less than 10% and this did not increase in response to arsenic (Fig.
240 4B). Statistical analysis of the 0 hr and 6 hr time-points data revealed that there was
241 a substantial and statistically significant recruitment of p97 to PML bodies in cells

242 expressing WT YFP-PMLV, but not in cells expressing A216T or L217F YFP-PMLV
243 (Fig. 4C). Changes in the expression levels of p97 in the different cell lines, or upon
244 arsenic treatment could not explain these differences (Supplementary Fig. 5). Thus,
245 although L217F YFP-PMLV recruits SUMO and RNF4 to generate ubiquitin
246 conjugates, this signal is somehow not sufficient to engage p97, and therefore
247 proteasomal degradation fails.
248
249 **Differential modification with SUMO and ubiquitin of PML mutants**
250 To provide more detail on the post-translational modifications that accumulate on
251 PML, we repeated the purification of YFP-PML nuclear bodies with a view to release
252 SUMO or ubiquitin from resin-bound material by treatment with proteases specific for
253 each (Supplementary Fig. 6A). The material released by protease treatment, and that
254 remaining on the beads can be analysed by Western blotting, which should provide
255 information not only on the covalent modification status of PML, but also that of the
256 SUMO1, SUMO2/3 and ubiquitin species attached to PML (Supplementary Fig. 6B).
257 Prior to purification, nuclear extracts for WT, A216T and L217F YFP-PMLV displayed
258 the expected changes in electrophoretic mobility (Supplementary Fig. 6C), and were
259 almost completely depleted from nuclear extracts after YFP-PML purification.
260 Importantly, the modifications to PML were preserved during purification (Fig. 5A “No
261 protease”). For all PML variants treatment of the beads with SENP1 returned most of
262 the heavier PML forms back to more rapidly migrating species consistent with
263 unmodified YFP-PMLV (Fig. 5 “SENP1” lanes). Treatment with USP2 had little impact
264 on the distribution of PML species, indicating only a relatively small proportion of the
265 modified PML is ubiquitin conjugated (Fig. 5A “USP2”). SUMO1 blots show that in
266 untreated cells there are relatively low levels of SUMO1 associated with PML, while

267 after arsenic treatment this increases dramatically for WT YFP-PMLV, modestly for
268 L217F YFP-PMLV, and not at all for A216T YFP-PMLV (Fig. 5B). As expected, these
269 species disappear upon SENP1 treatment, but are largely unaltered by treatment with
270 USP2 (Fig. 5B). After arsenic exposure, the relative increase to SUMO2/3 modification
271 is not as large as for SUMO1. Notably all three PML forms undergo an increase in
272 SUMO2/3 conjugation, although A216T PML is modified to a much lesser degree than
273 either WT or L217F (Fig. 5C). SUMO2/3 is also completely removed by SENP1, but
274 USP2 treatment does not result in significant changes to SUMO2/3 antibody reactive
275 species (Fig. 5C). Blotting with an antibody to ubiquitin reveals that it is present at low
276 levels on WT, A216T and L217F YFP-PMLV in untreated cells but is dramatically
277 increased on WT, modestly increased on L217F but any increase on A216T is
278 undetectable in this assay (Fig. 5D). For both WT PML and the L217F mutant, SENP1
279 treatment not only reduces the amount of ubiquitin remaining on the beads, it also
280 causes the ubiquitin-reactive species to run at a reduced molecular weight (Fig. 5D).
281 This ubiquitin released by SENP1 is probably conjugated directly to SUMO, while the
282 material remaining is directly conjugated to PML. As expected, ubiquitin is removed
283 from purifications by treatment with USP2 (Fig. 5D). Although ubiquitination of L217F
284 in response to arsenic is less than that of WT YFP-PMLV, it is still far more substantial
285 than the A216T mutant (Fig. 5D).

286 The material released from the bead-associated YFP-PMLV by treatment with the
287 proteases was also analysed by Western blotting. As expected, none of the treatments
288 released YFP-PMLV (Supplementary Fig. 7A). SENP1 treatment released low levels
289 of monomeric SUMO1 from untreated WT and L217F YFP-PMLV samples, with none
290 detected from A216T purifications. After arsenic treatment the amount of SUMO1
291 released by SENP1 from WT samples increased for both WT and L217F PML forms,

292 albeit less extensively for the mutant. Compared to these two, the amount of SUMO1
293 conjugated to A216T after arsenic exposure was negligible although it was at least
294 detectable compared to the sample derived from untreated cells (Supp. Fig. 7B).
295 SENP1 treatment of WT-PML purifications also released forms of SUMO1 shifted up
296 around 10kDa from the unmodified SUMO1 species, which are presumed to be
297 SUMO1 conjugated by ubiquitin, as they are sensitive to USP2 (Supplementary Fig.
298 7B). However, these species were not apparent in SENP1 elutions from L217F-PML
299 purifications according to this assay, implying ubiquitination of SUMO1 is most
300 extensive for in WT-PML. SENP1 digestion released substantial amounts of
301 monomeric SUMO2/3 from preparations derived from untreated cells for all PML
302 variants including A216T (Supp. Fig. 7C). Arsenic treatment induced a modest
303 increase in SUMO2/3 conjugates on all three PML forms, although a ubiquitinated
304 form of SUMO2/3 was only apparent for WT and L217F variants (Supp. Fig. 7C).
305 These SUMO-ubiquitin hybrid species released by SENP1 were also detected using
306 a ubiquitin antibody (Supplementary Fig. 7D). Although data shown in Fig. 5C suggest
307 SUMO2/3 modification of PML is low prior to arsenic and increases after arsenic
308 treatment, this is not consistent with analysis of the material released by SENP1
309 treatment (Supplementary Fig. 6C) which shows similar SUMO2/3 amounts both
310 before and after arsenic. A possible explanation for this apparent discrepancy is that
311 in untreated cells the SUMO2/3 modified PML are dispersed throughout the gel,
312 whereas after SENP1 treatment all the SUMO2/3 runs as a single species.

313 In summary, A216T YFP-PMLV is defective for arsenic induced SUMO1, SUMO2/3
314 and ubiquitin modification. L217F YFP-PMLV appears to be modestly compromised
315 for SUMO2/3 conjugation but shows much less than WT-PML levels of SUMO1
316 conjugation. Furthermore, WT PML shows higher levels of direct ubiquitination than

317 L217F, whereas L217F ubiquitination appears to mostly take place on SUMO2/3
318 linked to PML. Finally, a significant proportion of SUMO1 conjugated to WT-PML is
319 covalently conjugated by ubiquitin, while this was not detected for L217F PML.

320 **Quantitative proteomic analysis of PML post-translational modifications in**
321 **response to arsenic**

322 Early descriptions of PML modification by SUMO identified three major acceptors at
323 lysines 65, 160 and 490 (Kamitani, Kito et al. 1998). More recently, the single largest
324 SUMO site proteomic analysis to date (Hendriks, Lyon et al. 2017) described a total
325 of 15 acceptor lysines in PML (Supplementary figure 8A). To provide quantitative
326 data at the amino-acid site level for the post-translational modifications present in
327 PML and SUMO, a peptide-level quantitative proteomics analysis was undertaken.
328 Trypsin digestion leaves long SUMO adducts attached to modified lysines
329 (Supplementary Fig 8B), that are challenging to identify by mass-spectrometry. Thus,
330 a strategy combining GluC digestion and trypsin digestion was employed to give
331 shorter peptide fragments. As GluC is less specific and less stable than trypsin,
332 multiple GluC adducts from SUMOs remain on lysines after digestion
333 (Supplementary Fig. 8B), which has the advantage of providing multiple peptide
334 evidences for a single modification.
335 Cultures of U2OS PML-/- +YFP-PML cells were grown for the WT, A216T and L217F
336 PML variants, and were either treated or not with 1μM arsenic for 2 hr
337 (Supplementary Fig. 9A). Four experimental replicates for each condition were
338 prepared and YFP-PML purified by the same method as described above.
339 Purifications were analysed by SDS-PAGE (Supplementary Fig. 9B) and the
340 uppermost section of the gel containing proteins larger than 100kDa, including YFP-
341 PML, was processed for mass-spectrometry analysis. Anti-PML Western blot of a

342 fraction of the inputs revealed the YFP-PML proteins responded as expected to
343 arsenic treatment (Supplementary Fig. 9C). 21 phosphorylation, 14 SUMOylation
344 and 11 ubiquitination sites were identified in PML (Supplementary datafile 1 and
345 Supplementary Fig. 10A). Principal component analysis using intensity data for all
346 modified and unmodified peptides from YFP-PML, SUMO1, SUMO2, SUMO3 and
347 ubiquitin shows replicates cluster by experimental condition and are clearly
348 separated from one-another (Supplementary Fig. 10B), indicating consistent
349 differences among the conditions. Intensity data for all peptides were normalized by
350 total YFP peptide intensity (Supplementary Fig. 10C), to minimize any systematic
351 errors relating to PML expression or loading (Supplementary Fig. 10D). Using the
352 total intensity of the unmodified peptides from SUMO1, SUMO2/3 and ubiquitin as a
353 proxy for their overall protein abundance (Supplementary Fig. 10E-G), a remarkably
354 similar picture to that revealed in the Western blot experiments above (Fig. 3) was
355 found. Namely, prior to exposure to arsenic all three PML forms are associated with
356 broadly similar amounts of SUMO1, SUMO2/3 and ubiquitin. Arsenic treatment has
357 little effect on the modification of the A216T mutant, but triggers increased
358 conjugation by SUMO1, SUMO2/3 and ubiquitin for WT and L217F PML, with the
359 mutant showing a weaker response in SUMO1 and ubiquitin conjugation. Also
360 consistent with the Western blot data is the finding that SUMO1 has a larger relative
361 increase (5 fold) than SUMO2/3 (1.8 fold) in conjugation to WT PML after arsenic
362 treatment. To more easily compare multiple protein/peptide intensities, each
363 normalized intensity can be represented relative to the average intensity across all
364 samples (Supplementary Fig. 10H), which can then be plotted in a single compact
365 radial chart to show which differ the most between cell types and treatments
366 (compare with Fig. 6A).

367

368 **Site-specific differences in SUMO modification to PML mutants**

369 10 SUMO1 modifications to PML had reliable enough data for comparisons among
370 conditions (Fig. 6B). After arsenic treatment, WT PML was much more extensively
371 modified with SUMO1 than either mutant at all PML sites except K160 in B-Box1,
372 which appeared to be more occupied by SUMO1 in the L217F mutant (Fig. 6B). Site-
373 level analysis confirmed A216T PML was relatively unresponsive in SUMO1
374 conjugation. The results for SUMO2/3 were less clear-cut (Fig. 6C). Firstly, the scale
375 of the difference among the three PML forms in the SUMO2 conjugation is much
376 smaller than for SUMO1. Surprisingly, two of the 12 sites with good enough data for
377 quantitative comparisons were most highly modified in the apparently inert A216T
378 mutant (Fig. 6C). These were K226 close to the mutation hotspot and K487 in the
379 NLS (Fig. 6C). Several other sites in or around the NLS, K400, K476, and K497,
380 showed greater modification for L217F than WT PML (Fig. 6C). The WT protein only
381 showed the most extensive SUMO2/3 modification at K380 (between the coiled-coil
382 and NLS) and marginally higher conjugation at three sites; K65 (RING domain),
383 K426 and K460 (both between the coiled-coil and the NLS). Site-level analysis of
384 SUMO-SUMO branched peptides showed again that A216T PML was almost
385 completely unresponsive (Fig. 6D). SUMO polymers did accumulate on L217F PML,
386 but not to the same extent as for WT PML (Fig. 6D). Notably all bar one of the
387 identified SUMO-SUMO linages contained SUMO1 as conjugate donor, acceptor, or
388 both. Together these results show the higher levels of SUMO1 recruitment to WT
389 PML compared to the mutants was via direct conjugation to PML, as well as
390 SUMO1-SUMO polymer formation. Differences among the PML variants for SUMO2
391 conjuagation were more subtle and site-specific.

392

393 **Neither A216T nor L217F PML accumulate polyubiquitin chains in response to**
394 **arsenic**

395 Of the 11 ubiquitination sites identified in PML, the majority were sites also identified
396 as SUMO acceptors, except K183 between B-Boxes 1 and 2 and K337 in the coiled-
397 coil domain. 9 sites had high quality quantitative data which showed that A216T did
398 not respond to arsenic with increased ubiquitination at any site (Fig. 6E). In general
399 WT and L217F PML showed similar global increases in ubiquitination on PML
400 although there were differences at the site level. Notably both A216T and L217F
401 PML were much more highly modified at lysines 160 and 490 than WT (Fig. 6E).
402 These are two of the three sites originally identified as major SUMO acceptors, and
403 likely to already have relatively high occupancy with SUMO. K183 and K337 were
404 more occupied by ubiquitin in WT PML than either mutant (Fig. 6E). There is a
405 striking difference between WT and L217F in the ubiquitination of the associated
406 SUMO (Fig. 6F). 4 of the 5 ubiquitination sites in SUMO 1 and SUMO2/3 quantified
407 were more extensively ubiquitinated in L217F PML purifications then the WT
408 equivalent (Fig. 6F). Conversely, ubiquitin-ubiquitin conjugations were generally
409 more abundant in WT PML purifications than for L217F PML (Fig. 6G). These results
410 show that compared with WT PML, arsenic-induced ubiquitination of L217F PML is
411 skewed towards SUMO ubiquitination, and away from ubiquitin-ubiquitin polymer
412 formation.

413

414 **SUMO1 is essential for arsenic-induced PML degradation**

415 The finding that the stable L217F PML mutant is more defective in SUMO1
416 conjugation than SUMO2 is unexpected. RNF4 has been shown to have specificity

417 for polymeric SUMO conjugates, with a chain of 4 or more SUMOs having higher
418 affinity for RNF4 than shorter polymers or monomeric SUMO conjugates (Tatham,
419 Geoffroy et al. 2008). Due to the presence of an internal SUMO conjugation
420 consensus motif in SUMO2/3 but not SUMO1, it is assumed that SUMO2/3 form
421 branched conjugates more readily than SUMO1, and therefore represent the more
422 common RNF4 substrate. However, SUMO1 can still participate in polySUMO
423 conjugates as a SUMO donor, and proteomics studies have also found SUMO1 to
424 be an acceptor for SUMOylation, although the salience of this is poorly understood.
425 To investigate the role of SUMO1 in arsenic-induced PML degradation, a U2OS cell
426 line lacking SUMO1 (SUMO1 -/- U2OS) was generated by CRISPR-cas9 genome
427 editing. Immunofluorescence confirmed the loss of SUMO1 expression in these cells
428 (Fig. 7A). Anti-PML Western-blot analysis of crude cell extracts of cells exposed to
429 1μM As over 24 hr showed that in cells lacking SUMO1 there is a molecular weight
430 shift in PML in a manner similar to SUMO1 +/+ cells (Fig. 7B), but the modified forms
431 of PML appear to be more resistant to degradation. These persist up to 24 hr after
432 addition of As to the medium, when PML from WT cells is almost completely
433 degraded (Fig. 7B). Furthermore, after these extended periods of As exposure,
434 unconjugated PML begins to re-accumulate in SUMO1 - / cells (Fig. 7C), almost
435 returning the cellular pool of PML to the initial state (Compare 0h and 24h lanes in
436 Fig. 7C). This confirms SUMO1 is essential for PML degradation and insufficient
437 conjugation of the L217F PML mutant by SUMO1 potentially explains its stability
438 during arsenic exposure.
439
440 **DISCUSSION**

441 The overarching cellular mechanisms governing arsenic-induced degradation of PML
442 and the oncogenic fusion PML-RARA were broadly characterised more than ten
443 years ago (Lallemand-Breitenbach, Jeanne et al. 2008, Tatham, Geoffroy et al.
444 2008). Arsenic triggers the SUMOylation of PML, followed by its ubiquitination, then
445 degradation by the proteasome. However, the precise molecular signals and effector
446 proteins required to progress through each step are not fully understood. The
447 functional characterisation of mutant forms of PML and PML-RAR found in APL
448 patients refractory to arsenic treatment, provides an opportunity to better understand
449 the biochemical details of arsenic-induced PML degradation by understanding their
450 loss of function. We have used a combination of high content, time-lapse
451 microscopy, and peptide-level proteomic analysis to study two common patient-
452 derived PML mutants; A216T and L217F. We generated three model U2OS cell lines
453 lacking endogenous PML but expressing YFP fusions of WT PML, A216T PML or
454 L217F PML. In untreated cells the two mutants of PML formed atypical nuclear
455 bodies, fewer in number and larger in size than WT bodies, and both mutants were
456 stable when cells were exposed to 1μM arsenic for 24 hours. Importantly, during
457 arsenic treatment the modification status of each was quite different, and both
458 differed from WT PML.
459 After 2 hours exposure to 1μM arsenic, A216T PML appeared almost inert and
460 showed little increase in either SUMOylation or ubiquitination. Thus, A216T PML
461 stability is explained by a failed SUMOylation response early in the degradation
462 pathway. In contrast, arsenic did trigger SUMO and ubiquitin conjugation to L217F
463 PML, and yet it was not degraded. Site level proteomics revealed that while
464 ubiquitination did increase for L217F PML, it differed from WT PML in the precise
465 lysine sites to which it conjugated. The ubiquitin associated with L217F appeared to

466 favour attachment to SUMO molecules, while on WT-PML ubiquitin accumulated
467 more in polyubiquitin chains. This lack of polyubiquitin chain formation potentially
468 explains the observed lack of recruitment to L217F-PML of the segregase p97, which
469 recognises ubiquitin chains and is essential for PML degradation (Jaffray, Tatham et
470 al. 2023). p97 recognises polyubiquitin chains containing 5 or more copies of
471 ubiquitin (Twomey, Ji et al. 2019), and both K11 and K48 linkages are implicated in
472 p97 function (Locke, Toth et al. 2014, Meyer and Rape 2014, Yau, Doerner et al.
473 2017). Crucially, WT-PML showed statistically significant increases in ubiquitin-
474 ubiquitin linkages via K11, K33 and K48 (Supp. Fig. 11A). Although these increases
475 were modest, we expect an appropriate degradation signal for PML to be short-lived
476 in cells, making their detection difficult in studies like these.
477 Arsenic exposure triggered a much greater SUMO1 response on WT PML than it did
478 for SUMO2/3. From these studies we cannot determine whether more SUMO1 than
479 SUMO2/3 was conjugated to PML, but relative to initial conjugation levels, the
480 SUMO1 response was much greater than SUMO2/3. Furthermore, the L217F mutant
481 displayed lower levels of SUMO1 conjugation upon arsenic exposure than WT PML,
482 while total amounts of SUMO2/3 associated with both PML forms were comparable.
483 The importance of SUMO1 was further evidenced by the finding that WT PML is
484 stable in cells lacking SUMO1, suggesting that SUMO2/3 cannot compensate for its
485 loss. This raises the possibility that sub-optimal SUMO1 conjugation may lead to the
486 failure of L217F to generate the appropriate ubiquitin signal for p97 binding.
487 Based on the current model for PML degradation, critical requirement for SUMO1
488 seems counter intuitive. The E3 ligase responsible for PML ubiquitination, RNF4 is
489 poly-SUMO specific (Tatham, Geoffroy et al. 2008), and by lacking an internal
490 SUMO conjugation consensus, SUMO1 is thought not to form polySUMO chains as

491 readily as SUMO2/3. Incorporation of SUMO1 into SUMO2/3 polymers could
492 suppress further polymer formation by blocking lysines in SUMO2/3, and so SUMO1
493 may be expected to be inhibitory to PML degradation via RNF4. One potential
494 explanation is enough SUMOs in close proximity could substitute for a SUMO
495 polymer, and engage and activate RNF4 (Aguilar-Martinez and Sharrocks 2016).
496 This may be more likely for a protein like PML which forms multimeric complexes
497 and contains numerous SUMOylation sites. It is also conceivable that independent of
498 RNF4, SUMO1 provides a unique signal recognised by an as-yet unidentified protein
499 effector of the PML degradation pathway that specifically recognises SUMO1 and
500 not SUMO2/3. These prospects will require further investigation.
501 Alternatively, rather than generating a new signal, SUMO-1 may function to suppress
502 the formation of unproductive signals. For example SUMO1 may compete with
503 ubiquitin for conjugation to lysine residues on proteins other than ubiquitin itself, and
504 so promote polyubiquitin chain formation. In this way SUMO1 modification of lysines
505 from SUMOs attached to WT-PML or PML itself may block spurious ubiquitination
506 and effectively drive the synthesis of ubiquitin-ubiquitin linkages required for
507 degradation. L217F PML which is less SUMO1 modified than WT-PML might then
508 have more available non-ubiquitin lysines and so does not synthesise ubiquitin
509 chains as readily. Consistent with this, ubiquitination of SUMOs was found to be
510 generally higher for L217F PML than WT (Fig. 6F), and SUMO1-SUMO linkages
511 were more abundant in WT-PML preps than L217F (Fig. 6D).
512 In summary, two patient-derived mutant forms of PML, A216T and L217F result in
513 similar clinical aetiologies but have subtly different biochemical responses to arsenic
514 resulting in blocked degradation (See Supplementary figure 12). A216T is almost
515 completely unresponsive to arsenic, experiencing only very modest changes in

516 SUMOylation and ubiquitination, most likely because it does not engage the
517 appropriate SUMO conjugation machinery. L217F PML does become modified with
518 both SUMO1 and SUMO2/3, but while ubiquitination is stimulated, it does not create
519 the appropriate signal required to recruit p97 prior to degradation by the proteasome.
520 These results reveal the subtle intricacies of the PML degradation pathway, and
521 propose a higher level of complexity than previously considered.
522

523 **MATERIALS AND METHODS**

524 **Preparation of anti-GFP nanobody magnetic beads.** 300mg of Dynabeads M-270
525 Epoxy (ThermoFisher Scientific Catalogue No. 14302D) were resuspended in 10 ml
526 of 0.1 M sodium phosphate buffer pH 7.5 and washed twice using a DynaMag-15
527 magnet (ThermoFisher Scientific Catalogue No. 12301D) with 10 ml of the same
528 buffer. 4 mg of the LaG16 nanobody that recognises GFP (Fridy, Li et al. 2014) in 10
529 ml of 1 M $(NH_4)_2SO_4$, 0.1 M sodium phosphate buffer pH 8.0 was added to the beads
530 which were incubated overnight at 27ºC with end over end rotation. After coupling was
531 complete the beads were washed 6 times with phosphate buffered saline (PBS) and
532 stored in PBS, 0.1% NaN_3 at 4^0C.
533

534 **Purification of YFP-PML from U2OS PML-/- YFP-PML cells.** For each 'replicate' of
535 the proteomics experiment five 15 cm diameter plates of approximately 80% confluent
536 cells were used. Prior to harvesting, growth medium was removed and cells washed
537 in situ twice with 5mL PBS/100mM iodoacetamide. For each dish, cells were scraped
538 into 5mL PBS+100mM iodoacetamide and transferred to a 50mL tube. A second 2mL
539 volume of PBS+100mM iodoacetamide was used to clean the plate of all cells and
540 pooled with the first 5mL. This was repeated for all dishes for each replicate and

541 pooled in the same 50mL tube (~35mL total). Cells were pelleted by centrifugation at
542 400g for 5 minutes at 22ºC and resuspended in 10 mL 4ºC hypotonic buffer including
543 iodoacetamide (10mM HEPES pH 7.9, 1.5mM MgCl2, 10mM KCl, 0.08% NP-40, 1x
544 EDTA-free protease inhibitor cocktail (Roche), + 100mM Iodoacetamide). A sample of
545 this may be retained as a "Whole cell extract". These were snap-frozen in liquid
546 nitrogen and stored at -80ºC until required. Cells were thawed by tube rotation at 4ºC
547 for 30 minutes. Tubes were then centrifuged at 2000g, 4ºC for 10 minutes to pellet
548 nuclei. Supernatants were discarded but a sample of this can be taken as a "Cytosolic
549 fraction". Each pellet of nuclei was resuspended in 5mL ice-cold hypotonic buffer
550 containing 20mM DTT but without iodoacetamide, transferred to a 15mL tube and
551 centrifuged at 2000g, 4ºC for 10 minutes. The nuclei were washed once more in 5mL
552 ice-cold hypotonic buffer (without iodoacetamide or DTT) and the supernatant
553 discarded. To digest DNA, nuclei were resuspended in 5mL "Buffer A" (50mM Tris pH
554 7.5, 150mM NaCl, 0.2mM DTT, 1µg/ml benzonase, 1x EDTA-free protease inhibitor
555 cocktail (Roche)) and incubated on ice for 15 minutes. Samples were sonicated in
556 15mL tubes on ice (Branson Sonifier) using the small probe, 6 cycles of 30 seconds
557 at approximately 50% amplitude with at least 2 minutes cooling on ice in between
558 cycles. PML bodies should remain intact at this point. Insoluble debris was removed
559 by centrifugation at 1200g for 20 minutes at 4ºC, and the supernatant containing
560 soluble PML bodies, transferred to a new 15ml centrifuge tube. A sample of this can
561 be taken as a "Nuclear fraction". To each 5mL supernatant 6mL "Buffer B" was added
562 (50mM Tris pH 7.5, 1% Triton-X-100, 0.1% Deoxycholic acid, 1x EDTA-free protease
563 inhibitor cocktail (Roche)). To each 11mL solution, 1mL volume of a 5% beads:buffer
564 slurry (v:v) of magnetic anti-GFP nanobody beads, pre-equilibrated in 1:1.4 Buffer A:B
565 mix (v:v), was added and mixed on a tube roller at 4ºC for 16h (50µL beads per

566 sample). Using the DynaMag rack (Thermofisher scientific) the beads were extracted
567 from suspension and the supernatant removed. A sample of this can be analysed to
568 ensure YFP-PML depletion. Beads were then washed with 5mL “Buffer C” (50mM Tris
569 pH 7.5, 500mM NaCl, 0.2mM DTT) and the beads extracted. These beads were then
570 resuspended in 1mL “Buffer D” (50mM Tris pH 7.5, 150mM NaCl, 0.2mM DTT) and
571 transferred to a new 1.5mL protein LoBind tube (Eppendorf) and after bead separation,
572 washed once more with 1mL Buffer D. One half of this final sample of beads (25μL
573 beads) was eluted for proteomic analysis by adding 35µl 1.2X NuPAGE LDS sample
574 buffer (Thermofisher scientific), and incubated at 70ºC for 15 minutes with agitation,
575 followed by fractionation by SDS-PAGE. If Western blot analysis was also required,
576 the second half of the resin (25μL) would be resuspended in 250µl 1.2X NuPAGE LDS
577 sample buffer (Thermo) and incubated at 70ºC for 15 minutes with agitation.
578 Approximately 30µl would be used per gel lane. If treatment with proteases was
579 required to monitor PML modification status, then the second half volume of beads
580 (25μL) was divided into four and treated as follows: 1-Add 150 µl Buffer D. 2-Add 150
581 µl 250nM SENP1 in Buffer D. 3- Add 150 µl 500nM USP2 in Buffer D. 4- Add 150 µl
582 250nM SENP1/500nM USP2 in Buffer D. All tubes were agitated for 1-2 hrs at 22ºC,
583 supernatants removed (and can be kept for analysis) and beads washed twice with
584 1mL buffer D before elution with 250 µl 1.2X LDS, 70ºC, 15 minutes with agitation.
585
586 **Proteomic analysis of YFP-PML purifications.** Elutions from anti-GFP nanobody
587 beads in 1.2x LDS/60mM DTT protein sample buffer were fractionated on 4-12%
588 polyacrylamide Bis-Tris NuPAGE gels (Thermofisher Scientific) using MOPS running
589 buffer. After Coomassie staining and destaining gels were excised into 4 slices per
590 lane and tryptic peptides extracted from top slice (>100kDa) as previously described

591 (Shevchenko, Tomas et al. 2006). Peptides were resuspended in 40μL 0.1% TFA
592 0.5% acetic acid and half STAGE tip purified prior to digestion with GluC. This gave
593 two fractions per replicate: Trypsin digested, and Trypsin+GluC digested. 6μL of each
594 was analysed by LC-MS/MS. This was performed using a Q Exactive mass
595 spectrometer (Thermofisher Scientific) coupled to an EASY-nLC 1000 liquid
596 chromatography system (Thermofisher Scientific), using an EASY-Spray ion source
597 (Thermofisher Scientific) running a 75 µm x 500 mm EASY-Spray column at 45ºC. A
598 150 minute elution gradient with a top 8 data-dependent method was applied. Full
599 scan spectra (m/z 300–1800) were acquired with resolution R = 70,000 at m/z 200
600 (after accumulation to a target value of 1,000,000 ions with maximum injection time of
601 20 ms). The 8 most intense ions were fragmented by HCD and measured with a
602 resolution of R = 17,500 at m/z 200 (target value of 500,000 ions and maximum
603 injection time of 120 ms) and intensity threshold of 2.1×10^4. Peptide match was set to
604 'preferred', a 40 second dynamic exclusion list was applied and ions were ignored if
605 they had unassigned charge state 1, 8 or >8.
606 MS data were processed in MaxQuant version 1.6.1.0 (Cox and Mann 2008, Cox,
607 Neuhauser et al. 2011). Multiple MaxQuant runs were performed considering multiple
608 SUMO1 and SUMO2/3 derived adducts as variable modifications (see Supplementary
609 Datafile 1 for details), as well as those typical for ubiquitin and phosphorylation to Ser
610 and Thr residues. A MaxQuant search for SUMO adducts was also conducted using
611 a concatenated database approach using linear peptide fusions of SUMO C-termini to
612 substrate peptides as search library (Matic, van Hagen et al. 2008). Oxidised
613 methionine and acetylated protein N-termini were also selected as variable
614 modifications and carbamidomethyl-C was the only fixed modification. Maximum
615 number of variable modifications was set to 4. The match between runs option was

616 enabled, which matches identified peaks among slices from the same position in the
617 gel as well as one slice higher or lower. The uniport human proteome database
618 (downloaded 19/4/2019 - 73920 entries) digested with Trypsin/P (maximum missed
619 cleavages was 5) was used as search space. LFQ intensities were required for each
620 slice. All FDR filtering was set to 1%. For peptides derived from GluC digestions 8
621 maximum missed cleavages were considered. Raw peptide intensities were manually
622 normalized by the total YFP peptide intensity for each sample. Mass spectrometry
623 data from samples derived from the same replicate were numerically summed to
624 provide a final normalized peptide intensity for each identification in each sample.
625 Downstream data processing used Perseus v1.6.1.1 (Tyanova, Temu et al. 2016).
626 Zero intensity values were replaced from $\log_2$ transformed data (width 0.3 and
627 downshift 1.8).
628
629 **Pre-extraction of cells**. Cells were grown on coverslips in 24 well plates. Coverslips
630 were washed twice with PBS before being exposed to pre-extraction buffer (25 mM
631 HEPES pH 7.4, 50 mM NaCl, 3 mM MgCl2, 0.5% Triton-X-100, 0.3M Sucrose) for 10
632 min. Cells were then processed through the procedure below for immunofluorescence.
633
634 **Immunofluorescence analysis.** Adherent cells were washed three times with PBS,
635 fixed with 4% Formaldehyde in PBS for 15mins, then washed again three times with
636 PBS before blocking for 30 min in 5% BSA, 0.1% TWEEN 20 in PBS. Fixed cells were
637 washed once with 1% BSA, 0.1% TWEEN 20 in PBS before incubation for 1-2 hr with
638 primary antibody in 1% BSA, 0.1% TWEEN 20 in PBS. These were chicken anti-PML
639 (in house) and sheep anti-p97 (MRC Dundee). After 3 washes in 1% BSA, 0.1%
640 TWEEN 20 in PBS cells were incubated with secondary antibody in 1% BSA, 0.1%

641 TWEEN 20 in PBS for 60 min., washed three times in 1% BSA, 0.1% TWEEN 20 in
642 PBS and stained with 0.1µg/ml DAPI for 2 min. These were Alexa Fluor (Invitrogen)
643 Donkey anti-chicken 594, donkey anti-sheep 594 and donkey anti-chicken 488. Cover
644 slips were rinsed twice with PBS, twice with water and dried before mounting in
645 MOWIOL. Images were collected using a DeltaVision DV3 widefield microscope and
646 processed using Softworx (both Applied Precision, Issaquah, WA). Images are
647 presented as maximal intensity projections using Omero software. For quantitative
648 p97-PML colocalization analysis the same image settings were applied across all
649 fields and PML bodes per cell were counted for between 20 and 40 cells per condition.
650 P97 colocalisation was defined as any p97 signal above background within the same
651 region as a PML body. Percent colocalization was then calculated for each cell.
652
653 **Live-Cell Imaging in Real Time and Measurement of Fluorescence Intensities.**
654 For all live-cell imaging experiments, cells were seeded onto µ-slide 8 well glass
655 bottom (Ibidi 80827). Immediately prior to imaging cell medium was replaced with
656 DMEM minus phenol red (gibco 31053-038) supplemented with 2mM glutamine and
657 10% fetal bovine serum. Cells were untreated or treated with 1µM arsenic. Time-laspe
658 microscopy was performed on a DeltaVision Elite restoration microscope (Cytiva)
659 fitted with an incubation chamber (Solent Scientific) set to 37 ºC and 5% CO2 and a
660 cooled charge-coupled device camera (CoolSnap HQ; Roper). SoftWorx software was
661 used for image collection. Datasets were deconvolved using the constrained iterative
662 algorithm (Swedlow, Sedat et al. 1996, Wallace, Schaefer et al. 2001) using SoftWorx
663 software. Using a YFP specific filter set (Ex510/10nm, Em537/26nm), 5 z-planes
664 spaced at 2 µm were taken every 15 min. A single brightfield reference image was
665 taken at each time point to monitor cell health. Time courses were presented as

666 maximum intensity projections of deconvolved 3D datasets. Movies were created in
667 OMERO using the deconvolved images.
668
669 **Quantitative analysis of PML body composition during Live-Cell imaging**
670 Batch analysis of time-lapse movies was carried out using ImageJ (Schneider,
671 Rasband et al. 2012) macros in Fiji (Schindelin, Arganda-Carreras et al. 2012)
672 (Supplementary Materials). Briefly: 1) datasets (deconvolved with SoftWoRx) were
673 cropped to remove border artefacts, 2) for each timepoint the maximum focus slice
674 was selected according to intensity variance (radius 2 pixels), 3) auto-thresholding
675 was performed using a threshold of mean intensity + 3 standard deviations, and 4)
676 ImageJ's built-in "Analyze Particles" function was used to measure PML body count,
677 size, total area, and intensity. Results were aggregated and summarized using R
678 scripts as described previously (Jaffray, Tatham et al. 2023).
679
680 **Preparation of cell extracts and Western blotting.** Adherent cells were washed with
681 PBS and lysed by the addition of 1.2X LDS buffer and heated to 70ºC for 10 min. Cell
682 lysates were sonicated using a probe sonicator for two bursts of 30 sec. Samples were
683 run on NuPage 3-8% or 4-12% Bis-Tris precast gels (ThermoFisher Scientific) and
684 transferred to nitrocellulose. Membranes were blocked in PBS with 5% non-fat milk
685 and 0.1% Tween-20. Primary antibody incubations were performed in PBS with 3%
686 BSA and 0.1% Tween-20. For the HRP-coupled secondary antibody incubations 5%
687 milk was used instead of the BSA. The signal was detected by Pierce enhanced
688 chemiluminescence (ThermoFisher scientific 32106) and X-ray films. Antibodies.
689 Chicken anti-PML (homemade), sheep anti-SUMO-1 (homemade), rabbit anti-SUMO-
690 2 (Cell signaling 4971S), rabbit FK2 ubiquitin (Enzo BML-PW8810-0500), rabbit anti-

691 p97 (Abcam ab109240). HRP-coupled secondary anti-mouse, anti-rabbit anti-chicken
692 and anti-sheep were purchased from Sigma.
693
694 **FIGURE LEGENDS**
695 **Figure 1. Characterization of PML bodies in U2OS PML-/- cell lines expressing**
696 **YFP-fusions of WT, A216T and L217F forms of PML-V.** A. Schematic depiction of
697 PML-V primary structure indicating the major domains, regions of common mutations
698 associated with arsenic treatment resistance, and the common breakpoints leading
699 to PML-RARA fusions. B. Representative images of the indicated PML-/- U2OS +
700 YFP-PML-V cell lines C. High content imaging data summarizing the calculated
701 values for total PML intensity per cell, PML body number per cell and area per PML
702 body for each cell line. Scatter plots are shown with median (solid line) and quartiles
703 (error bars). n=38411 (wt), 35210 (A216T) and 41288 (L217F).
704
705 **Figure 2. A216T and L217F mutants of PML are not rapidly degraded in**
706 **response to arsenic treatment in vitro.** A. YFP fluorescence image stills from one
707 live cell analysis of each YFP-PML cell type at both 0h and 15h treatment with 1μM
708 arsenic. B. Averaged data of 9 or 10 fields of view (median 12 cells per field)
709 followed over a 15 hour time course of treatment or not with 1μM arsenic (15 minute
710 intervals). Intensity measurements are normalized by the t=0hr values. C. Summary
711 statistics (n=9 or 10) for 15hr data comparing 1μM arsenic treated cells with
712 untreated cells. P-values are unpaired, two-tailed student's T-tests using Welch's
713 correction for unequal variances where appropriate (§). See Supplementary movie
714 files 1-6 for real-time data of a single representative field. D. Anti-PML Western-blots

715 of fractionated whole cell extracts showing time-courses of the response of YFP-
716 PML-V variants to 1μM arsenic exposure over 24 hours.
717
718 **Figure 3. In response to arsenic A216T PML fails to recruit RNF4.** Two separate
719 purifications of YFP-PMLV WT, A216T and L217F (A+B): PML bodies were enriched
720 from U2OS PML-/- + YFP-PMLV WT, A216T or L217F cells, either nontreated (NT)
721 or treated with 1μM arsenic (1μM As 2h) for 2 hr. Bound material was eluted and
722 analysed by Western blotting using antibodies to (A) PML, SUMO1, SUMO2/3 and
723 (B) PML, RNF4 and ubiquitin.
724
725 **Figure 4. A216T and L217F mutants of PML do not recruit p97 in response to**
726 **arsenic treatment.** A. Immunofluorescence images showing YFP-PMLV and p97 in
727 the indicated cell lines after 6 hours arsenic treatment. Data showing merged images
728 for these and the 0h time-point data can be seen in supplementary figure 4. B.
729 Quantitative summary of p97 colocalization with PML bodies in the indicated cell
730 lines during 0h, 2h, 4h and 6h arsenic exposure. Markers show average values and
731 error bars are standard error of the mean. C. Statistical analysis of the comparison
732 between 0h and 6h arsenic exposure for PML-p97 colocalization. Columns represent
733 average % colocalization, error bars are standard error of the mean, cell count is
734 shown in brackets below each column and student's two-tailed t-test p-values are
735 shown above.
736
737 **Figure 5. Failure of arsenic resistant mutants to generate the SUMO and**
738 **ubiquitin modified intermediates required for degradation.** PML bodies were
739 enriched from U2OS PML-/- + YFP-PMLV WT, A216T or L217F cells, either

740 untreated (-) or treated with 1μM arsenic (+) for 2 hr. Purified PML bodies bound to
741 anti-GFP nanobody magnetic beads were either untreated (No protease), treated
742 with SUMO specific protease (SENP1), treated with ubiquitin specific protease
743 (USP2) or a combination of both (USP2 + SENP1). Material remaining bound to the
744 beads after treatment was eluted and analysed by Western blotting using antibodies
745 to A. PML, B. SUMO1, C. SUMO2/3 and D. ubiquitin.
746
747 **Figure 6. Differential site-specific modifications of WT, A216T and L217F PML**
748 **forms before and after arsenic.** PML bodies were enriched from U2OS PML-/- +
749 YFP-PMLV WT, A216T or L217F cells and quantitatively analysed by mass
750 spectrometry for protein content and site-specific modifications by SUMO1,
751 SUMO2/3 and ubiquitin. A-G. Radial plots showing relative intensity for each of the
752 indicated proteins or peptides. A. is derived from the total of the unmodified peptides
753 for YFP, PML, SUMO1, SUMO2/3 and ubiquitin and is a proxy for of total protein
754 abundance. Circles indicate the upper limit of the range, with the maximum relative
755 intensity in brackets.
756
757 **Figure 7. Effect of SUMO1 deletion on arsenic-induced WT PML degradation.** A.
758 Wild-type (SUMO1 +/+) and SUMO1 knockout (SUMO1 -/-) U2OS cells were
759 exposed to 1μM As for 2 hours to allow SUMO1 recruitment to PML bodies, fixed
760 and double stained with DAPI and anti-SUMO1 (FITC) before image acquisition
761 using InCell analyser 2200 high-content imaging microscope and differential image
762 visualization by ImageJ software. B. SUMO1 +/+ and SUMO1 -/- U2OS cells were
763 exposed to 1μM As for the indicated periods before lysis and analysis by Western
764 blot for PML. C. As in B except only for SUMO -/- cells and with more time-points.

765

766 **Supplementary Figure 1. Arsenic-induced colocalisation of SUMO1 with WT,**
767 **A216T and L217F forms of YFP-PML.** Colocalisation of SUMO1 with WT, A216T
768 and L217F PML variants after 1μM arsenic treatment for 2h studied by fluorescence
769 microscopy. Scale bar is 10μm.

770

771 **Supplementary Figure 2. Arsenic-induced SUMO2/3 colocalisation with WT,**
772 **A216T and L217F forms of YFP-PML.** Colocalisation of SUMO2/3 with WT, A216T
773 and L217F PML variants after 1μM arsenic treatment for 2h studied by fluorescence
774 microscopy. Scale bar is 10μm.

775

776 **Supplementary Figure 3. Arsenic-induced RNF4 colocalisation with WT, A216T**
777 **and L217F forms of YFP-PML.** Colocalisation of RNF4 with WT, A216T and L217F
778 PML variants after 1μM arsenic treatment for 2h studied by fluorescence
779 microscopy. Scale bar is 10μm.

780

781 **Supplementary Figure 4. Arsenic-induced p97 colocalisation with WT, A216T**
782 **and L217F forms of YFP-PML.** Representative immunofluorescence images for
783 1μM arsenic treated YFP-PMLV cells at 0 hr and 6 hr. Monochrome images for YFP-
784 PML and p97 channels are shown along with the merge of YFP-PMLV (green) and
785 p97 (red) with DAPI (blue).

786

787 **Supplementary Figure 5. p97 expression levels do not differ between cell types**
788 **or upon arsenic treatment.** Western blots for p97 and PML of whole cell extracts
789 from the indicated cell lines either treated or not with arsenic.

790

791 **Supplementary Figure 6. Treatment of purified PML bodies with recombinant**
792 **SUMO and Ubiquitin proteases reveals the nature of PML post-translational**
793 **modifications.** A. Overview of the experimental design for detection of ubiquitin and
794 SUMO conjugated to PML. B. Anti-PML Western blot for nuclear extracts from the
795 indicated cell lines before and after purification of YFP-PML with GFP nanobody
796 beads. C. Schematic depiction of the contents of YFP-PML bound to beads and
797 resulting supernatants after treatment with specific proteases.

798

799 **Supplementary Figure 7. Western blot analysis of the material eluted by SENP1**
800 **and USP2 from the purified YFP-PML forms indicated.** Associated with Figure 5.
801 Western blots using antibodies specific for PML (A), SUMO1 (B), SUMO2/3 (C) and
802 ubiquitin (D). 2ng standards of recombinant proteins (Rec.) were included with the
803 gels. The positions of recombinant PML (Rec.PML), unmodified forms of YFP-PML,
804 SUMO1, SUMO2 and ubiquitin are indicated, along with ubiquitinated species (*).

805

806 **Supplementary Figure 8. Known sites of PML SUMOylation and potential**
807 **peptide adducts remaining on substrates after trypsin and GluC digestion.** A.
808 Positions of previously identified SUMO conjugation sites relative to the structural
809 domains in PML. Isoform V is shown although identifications could be from other
810 isoforms. Data taken from Hendriks et al 2017 (Hendriks, Lyon et al. 2017). Common
811 breakpoints found in the PML-RARA and mutational hotspots found in arsenic
812 insensitive forms are indicated. B. Overview of the potential remnants of SUMO C-
813 termini attached to substrate lysine residues (K) when conjugates are cleaved by
814 Trypsin, or GluC considering multiple missed cleavages.

815

816 **Supplementary Figure 9. A proteomic study to quantitatively analyse arsenic-**
817 **induced changes to PML post-translational modifications at the site level.** A.
818 Overview of the proteomic experimental design. B. Coomassie-stained gel showing
819 the elutions from anti-GFP nanobody purifications for each replicate. Gel slices are
820 numbered. C. Anti-PML western blot of a fraction of the anti-GFP nanobody
821 purifications for each replicate.

822

823 **Supplementary Figure 10. Overview of the proteomic data for the post-**
824 **translational modification of PML WT, A216T and L217F**
825 A. Summary of SUMO and ubiquitin conjugation sites identified in this study. Region
826 of mutation hotspots is boxed. B. Principal component analysis of the quantitative
827 proteomic data using only peptides from YFP-PML, SUMOs or ubiquitin. These
828 included all unmodified peptides, phospho peptides, Ubiquitin branches and SUMO
829 branches on YFP-PML, SUMO1, SUMO2/3 and Ubiquitin. Total is 343 peptides and
830 uses $\log_2$ transformed and zero-replaced intensity values. C-G. Total unmodified
831 peptide intensity data for the indicted proteins. Bars are average intensities with
832 standard deviation error bars. p values are for two tailed student's t-test comparing
833 untreated with arsenic treated samples. n=4. H. Summary of the data shown in C-G
834 normalized by the average intensity for each protein.

835

836 **Supplementary Figure 11. Column plots of relative peptide intensity data for**
837 **selected peptide types.** A. Quantitative data for peptides indicative of Ubiquitin-
838 Ubiquitin linkages detected in the proteomics study. Columns are average values
839 with SD error bars. Student's t-test p-values are indicated.

840

841 **Supplementary Figure 12. Schematic summary of the arsenic-induced**
842 **responses of WT, A216T and L217F forms of PML.** WT, A216T and L217F forms
843 of PML are modified by broadly similar amounts of SUMO1 and SUMO2/3 in
844 untreated cells. Exposure of cells to arsenic triggers an increase in SUMO2/3
845 conjugation for WT PML and L217F PML, and a much smaller increase for A216T
846 PML. A large increase in SUMO1 conjugation is triggered for WT PML, with a
847 smaller increase for L217F PML, and no significant SUMO1 change for A216T.
848 Arsenic does not induce increased ubiquitination of A216T, while L217F experiences
849 increased ubiquitination to PML and SUMO proteins. WT PML also becomes
850 ubiquitinated on PML and SUMOs, but a fraction also forms ubiquitin-ubiquitin
851 polymers. Neither A216T PML nor L217F PML develop the requisite SUMO and/or
852 ubiquitin signals required to bind p97 and target them for degradation.

853

854 **REFERENCES**

855 Aguilar-Martinez, E. and A. D. Sharrocks (2016). "The Use of Multimeric Protein Scaffolds for
856 Identifying Multi-SUMO Binding Proteins." Methods Mol Biol **1475**: 195-204.
857 Alfonso, V., L. Iaccarino, T. Ottone, L. Cicconi, S. Lavorgna, M. Divona, R. Cairoli, A. Cristiano,
858 C. Ciardi, S. Travaglini, G. Falconi, S. K. Hasan, A. Venditti, W. Arcese, M. T. Voso and F. Lo-
859 Coco (2019). "Early and sensitive detection of PML-A216V mutation by droplet digital PCR in
860 ATO-resistant acute promyelocytic leukemia." Leukemia **33**(6): 1527-1530.
861 Balasundaram, N., S. Ganesan, E. Chendamarai, H. K. Palani, A. Venkatraman, A. A. Alex, S.
862 David, S. P. Kumar, N. R. Radhakrishnan, M. Yasar, S. Krishna, A. Korula, U. Kulkarni, N. B.
863 Janet, P. Balasubramanian and V. Mathews (2022). "Metabolic adaptation drives arsenic
864 trioxide resistance in acute promyelocytic leukemia." Blood Adv **6**(2): 652-663.
865 Bernardi, R. and P. P. Pandolfi (2007). "Structure, dynamics and functions of promyelocytic
866 leukaemia nuclear bodies." Nat Rev Mol Cell Biol **8**(12): 1006-1016.
867 Chendamarai, E., S. Ganesan, A. A. Alex, V. Kamath, S. C. Nair, A. J. Nellickal, N. B. Janet, V.
868 Srivastava, K. M. Lakshmi, A. Viswabandya, A. Abraham, M. Aiyaz, N. Mullapudi, R.
869 Mugasimangalam, R. A. Padua, C. Chomienne, M. Chandy, A. Srivastava, B. George, P.
870 Balasubramanian and V. Mathews (2015). "Comparison of newly diagnosed and relapsed
871 patients with acute promyelocytic leukemia treated with arsenic trioxide: insight into
872 mechanisms of resistance." PLoS One **10**(3): e0121912.

873 Cox, J. and M. Mann (2008). "MaxQuant enables high peptide identification rates,
874 individualized p.p.b.-range mass accuracies and proteome-wide protein quantification." Nat
875 Biotechnol **26**(12): 1367-1372.
876 Cox, J., N. Neuhauser, A. Michalski, R. A. Scheltema, J. V. Olsen and M. Mann (2011).
877 "Andromeda: a peptide search engine integrated into the MaxQuant environment." J
878 Proteome Res **10**(4): 1794-1805.
879 de The, H., C. Lavau, A. Marchio, C. Chomienne, L. Degos and A. Dejean (1991). "The PML-
880 RAR alpha fusion mRNA generated by the t(15;17) translocation in acute promyelocytic
881 leukemia encodes a functionally altered RAR." Cell **66**(4): 675-684.
882 Dyck, J. A., G. G. Maul, W. H. Miller, Jr., J. D. Chen, A. Kakizuka and R. M. Evans (1994). "A
883 novel macromolecular structure is a target of the promyelocyte-retinoic acid receptor
884 oncoprotein." Cell **76**(2): 333-343.
885 Fridy, P. C., Y. Li, S. Keegan, M. K. Thompson, I. Nudelman, J. F. Scheid, M. Oeffinger, M. C.
886 Nussenzweig, D. Fenyo, B. T. Chait and M. P. Rout (2014). "A robust pipeline for rapid
887 production of versatile nanobody repertoires." Nat Methods **11**(12): 1253-1260.
888 Geoffroy, M. C. and R. T. Hay (2009). "An additional role for SUMO in ubiquitin-mediated
889 proteolysis." Nat Rev Mol Cell Biol **10**(8): 564-568.
890 Goto, E., A. Tomita, F. Hayakawa, A. Atsumi, H. Kiyoi and T. Naoe (2011). "Missense
891 mutations in PML-RARA are critical for the lack of responsiveness to arsenic trioxide
892 treatment." Blood **118**(6): 1600-1609.
893 Grignani, F., P. F. Ferrucci, U. Testa, G. Talamo, M. Fagioli, M. Alcalay, A. Mencarelli, F.
894 Grignani, C. Peschle, I. Nicoletti and et al. (1993). "The acute promyelocytic leukemia-
895 specific PML-RAR alpha fusion protein inhibits differentiation and promotes survival of
896 myeloid precursor cells." Cell **74**(3): 423-431.
897 Hendriks, I. A., D. Lyon, C. Young, L. J. Jensen, A. C. Vertegaal and M. L. Nielsen (2017). "Site-
898 specific mapping of the human SUMO proteome reveals co-modification with
899 phosphorylation." Nat Struct Mol Biol **24**(3): 325-336.
900 Iaccarino, L., T. Ottone, V. Alfonso, L. Cicconi, M. Divona, S. Lavorgna, S. Travaglini, A.
901 Ferrantini, G. Falconi, C. Baer, M. Usai, F. Forghieri, A. Venditti, M. I. Del Principe, W. Arcese,
902 M. T. Voso, T. Haferlach and F. Lo-Coco (2019). "Mutational landscape of patients with acute
903 promyelocytic leukemia at diagnosis and relapse." Am J Hematol **94**(10): 1091-1097.
904 Iaccarino, L., T. Ottone, M. Divona, L. Cicconi, R. Cairoli, M. T. Voso and F. Lo-Coco (2016).
905 "Mutations affecting both the rearranged and the unrearranged PML alleles in refractory
906 acute promyelocytic leukaemia." Br J Haematol **172**(6): 909-913.
907 Jaffray, E. G., M. H. Tatham, B. Mojsa, M. Liczmanska, A. Rojas-Fernandez, Y. Yin, G. Ball and
908 R. T. Hay (2023). "The p97/VCP segregase is essential for arsenic-induced degradation of
909 PML and PML-RARA." J Cell Biol **222**(4).
910 Kakizuka, A., W. H. Miller, Jr., K. Umesono, R. P. Warrell, Jr., S. R. Frankel, V. V. Murty, E.
911 Dmitrovsky and R. M. Evans (1991). "Chromosomal translocation t(15;17) in human acute
912 promyelocytic leukemia fuses RAR alpha with a novel putative transcription factor, PML."
913 Cell **66**(4): 663-674.
914 Kamitani, T., K. Kito, H. P. Nguyen, H. Wada, T. Fukuda-Kamitani and E. T. Yeh (1998).
915 "Identification of three major sentrinization sites in PML." J Biol Chem **273**(41): 26675-
916 26682.
917 Kwok, C., B. B. Zeisig, S. Dong and C. W. So (2006). "Forced homo-oligomerization of
918 RARalpha leads to transformation of primary hematopoietic cells." Cancer Cell **9**(2): 95-108.

919 Lallemand-Breitenbach, V., M. Jeanne, S. Benhenda, R. Nasr, M. Lei, L. Peres, J. Zhou, J. Zhu,
920 B. Raught and H. de The (2008). "Arsenic degrades PML or PML-RARalpha through a SUMO-
921 triggered RNF4/ubiquitin-mediated pathway." Nat Cell Biol **10**(5): 547-555.
922 Lehmann-Che, J., C. Bally and H. de The (2014). "Resistance to therapy in acute
923 promyelocytic leukemia." N Engl J Med **371**(12): 1170-1172.
924 Liu, J., H. H. Zhu, H. Jiang, Q. Jiang and X. J. Huang (2016). "Varying responses of PML-RARA
925 with different genetic mutations to arsenic trioxide." Blood **127**(2): 243-250.
926 Lo-Coco, F., G. Avvisati, M. Vignetti, C. Thiede, S. M. Orlando, S. Iacobelli, F. Ferrara, P. Fazi,
927 L. Cicconi, E. Di Bona, G. Specchia, S. Sica, M. Divona, A. Levis, W. Fiedler, E. Cerqui, M.
928 Breccia, G. Fioritoni, H. R. Salih, M. Cazzola, L. Melillo, A. M. Carella, C. H. Brandts, E. Morra,
929 M. von Lilienfeld-Toal, B. Hertenstein, M. Wattad, M. Lubbert, M. Hanel, N. Schmitz, H. Link,
930 M. G. Kropp, A. Rambaldi, G. La Nasa, M. Luppi, F. Ciceri, O. Finizio, A. Venditti, F. Fabbiano,
931 K. Dohner, M. Sauer, A. Ganser, S. Amadori, F. Mandelli, H. Dohner, G. Ehninger, R. F.
932 Schlenk, U. Platzbecker, d. A. Gruppo Italiano Malattie Ematologiche, G. German-Austrian
933 Acute Myeloid Leukemia Study and L. Study Alliance (2013). "Retinoic acid and arsenic
934 trioxide for acute promyelocytic leukemia." N Engl J Med **369**(2): 111-121.
935 Locke, M., J. I. Toth and M. D. Petroski (2014). "Lys11- and Lys48-linked ubiquitin chains
936 interact with p97 during endoplasmic-reticulum-associated degradation." Biochem J **459**(1):
937 205-216.
938 Lou, Y., Y. Ma, J. Sun, X. Ye, H. Pan, Y. Wang, W. Qian, H. Meng, W. Mai, J. He, H. Tong and J.
939 Jin (2015). "Evaluating frequency of PML-RARA mutations and conferring resistance to
940 arsenic trioxide-based therapy in relapsed acute promyelocytic leukemia patients." Ann
941 Hematol **94**(11): 1829-1837.
942 Madan, V., P. Shyamsunder, L. Han, A. Mayakonda, Y. Nagata, J. Sundaresan, D. Kanojia, K.
943 Yoshida, S. Ganesan, N. Hattori, N. Fulton, K. T. Tan, T. Alpermann, M. C. Kuo, S. Rostami, J.
944 Matthews, M. Sanada, L. Z. Liu, Y. Shiraishi, S. Miyano, E. Chendamarai, H. A. Hou, G.
945 Malnassy, T. Ma, M. Garg, L. W. Ding, Q. Y. Sun, W. Chien, T. Ikezoe, M. Lill, A. Biondi, R. A.
946 Larson, B. L. Powell, M. Lubbert, W. J. Chng, H. F. Tien, M. Heuser, A. Ganser, M. Koren-
947 Michowitz, S. M. Kornblau, H. M. Kantarjian, D. Nowak, W. K. Hofmann, H. Yang, W. Stock,
948 A. Ghavamzadeh, K. Alimoghaddam, T. Haferlach, S. Ogawa, L. Y. Shih, V. Mathews and H. P.
949 Koeffler (2016). "Comprehensive mutational analysis of primary and relapse acute
950 promyelocytic leukemia." Leukemia **30**(12): 2430.
951 Martens, J. H., A. B. Brinkman, F. Simmer, K. J. Francoijs, A. Nebbioso, F. Ferrara, L. Altucci
952 and H. G. Stunnenberg (2010). "PML-RARalpha/RXR Alters the Epigenetic Landscape in
953 Acute Promyelocytic Leukemia." Cancer Cell **17**(2): 173-185.
954 Matic, I., M. van Hagen, J. Schimmel, B. Macek, S. C. Ogg, M. H. Tatham, R. T. Hay, A. I.
955 Lamond, M. Mann and A. C. Vertegaal (2008). "In vivo identification of human small
956 ubiquitin-like modifier polymerization sites by high accuracy mass spectrometry and an in
957 vitro to in vivo strategy." Mol Cell Proteomics **7**(1): 132-144.
958 Meyer, H. J. and M. Rape (2014). "Enhanced protein degradation by branched ubiquitin
959 chains." Cell **157**(4): 910-921.
960 Mi, J. Q., S. J. Chen, G. B. Zhou, X. J. Yan and Z. Chen (2015). "Synergistic targeted therapy
961 for acute promyelocytic leukaemia: a model of translational research in human cancer." J
962 Intern Med **278**(6): 627-642.
963 Mikesch, J. H., H. Gronemeyer and C. W. So (2010). "Discovery of novel transcriptional and
964 epigenetic targets in APL by global ChIP analyses: Emerging opportunity and challenge."
965 Cancer Cell **17**(2): 112-114.

Muller, S., M. J. Matunis and A. Dejean (1998). "Conjugation with the ubiquitin-related modifier SUMO-1 regulates the partitioning of PML within the nucleus." Embo J **17**(1): 61-70.

Perry, J. J., J. A. Tainer and M. N. Boddy (2008). "A SIM-ultaneous role for SUMO and ubiquitin." Trends Biochem Sci **33**(5): 201-208.

Rojas-Fernandez, A., A. Plechanovova, N. Hattersley, E. Jaffray, M. H. Tatham and R. T. Hay (2014). "SUMO chain-induced dimerization activates RNF4." Mol Cell **53**(6): 880-892.

Schindelin, J., I. Arganda-Carreras, E. Frise, V. Kaynig, M. Longair, T. Pietzsch, S. Preibisch, C. Rueden, S. Saalfeld, B. Schmid, J. Y. Tinevez, D. J. White, V. Hartenstein, K. Eliceiri, P. Tomancak and A. Cardona (2012). "Fiji: an open-source platform for biological-image analysis." Nat Methods **9**(7): 676-682.

Schneider, C. A., W. S. Rasband and K. W. Eliceiri (2012). "NIH Image to ImageJ: 25 years of image analysis." Nat Methods **9**(7): 671-675.

Shevchenko, A., H. Tomas, J. Havlis, J. V. Olsen and M. Mann (2006). "In-gel digestion for mass spectrometric characterization of proteins and proteomes." Nat Protoc **1**(6): 2856-2860.

Swedlow, J. R., J. W. Sedat and D. A. Agard (1996). Deconvolution in optical microscopy Deconvolution of Images and Spectra (2nd Ed). USA, Academic Press, Inc.**:** 284-309.

Tan, Y., X. Wang, H. Song, Y. Zhang, R. Zhang, S. Li, W. Jin, S. Chen, H. Fang, Z. Chen and K. Wang (2021). "A PML/RARalpha direct target atlas redefines transcriptional deregulation in acute promyelocytic leukemia." Blood **137**(11): 1503-1516.

Tatham, M. H., M. C. Geoffroy, L. Shen, A. Plechanovova, N. Hattersley, E. G. Jaffray, J. J. Palvimo and R. T. Hay (2008). "RNF4 is a poly-SUMO-specific E3 ubiquitin ligase required for arsenic-induced PML degradation." Nat Cell Biol **10**(5): 538-546.

Twomey, E. C., Z. Ji, T. E. Wales, N. O. Bodnar, S. B. Ficarro, J. A. Marto, J. R. Engen and T. A. Rapoport (2019). "Substrate processing by the Cdc48 ATPase complex is initiated by ubiquitin unfolding." Science **365**(6452).

Tyanova, S., T. Temu, P. Sinitcyn, A. Carlson, M. Y. Hein, T. Geiger, M. Mann and J. Cox (2016). "The Perseus computational platform for comprehensive analysis of (prote)omics data." Nat Methods **13**(9): 731-740.

Wallace, W., L. H. Schaefer and J. R. Swedlow (2001). "A workingperson's guide to deconvolution in light microscopy." Biotechniques **31**(5): 1076-1078, 1080, 1082 passim.

Wang, Z. Y. and Z. Chen (2008). "Acute promyelocytic leukemia: from highly fatal to highly curable." Blood **111**(5): 2505-2515.

Weis, K., S. Rambaud, C. Lavau, J. Jansen, T. Carvalho, M. Carmo-Fonseca, A. Lamond and A. Dejean (1994). "Retinoic acid regulates aberrant nuclear localization of PML-RAR alpha in acute promyelocytic leukemia cells." Cell **76**(2): 345-356.

Yau, R. G., K. Doerner, E. R. Castellanos, D. L. Haakonsen, A. Werner, N. Wang, X. W. Yang, N. Martinez-Martin, M. L. Matsumoto, V. M. Dixit and M. Rape (2017). "Assembly and Function of Heterotypic Ubiquitin Chains in Cell-Cycle and Protein Quality Control." Cell **171**(4): 918-933 e920.

Zhu, H. H., Y. Z. Qin and X. J. Huang (2014). "Resistance to arsenic therapy in acute promyelocytic leukemia." N Engl J Med **370**(19): 1864-1866.

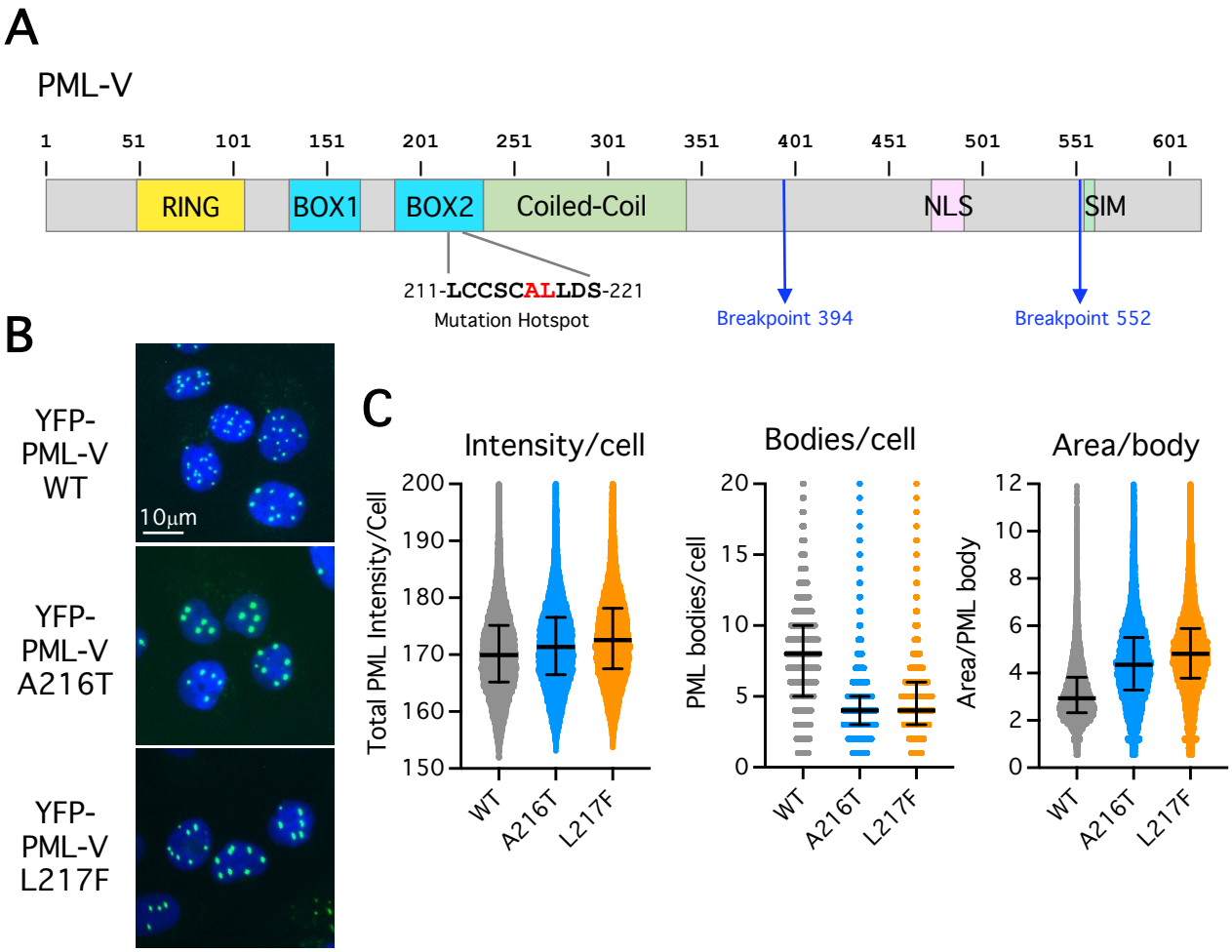

Figure 1. Jaffray et al 2023

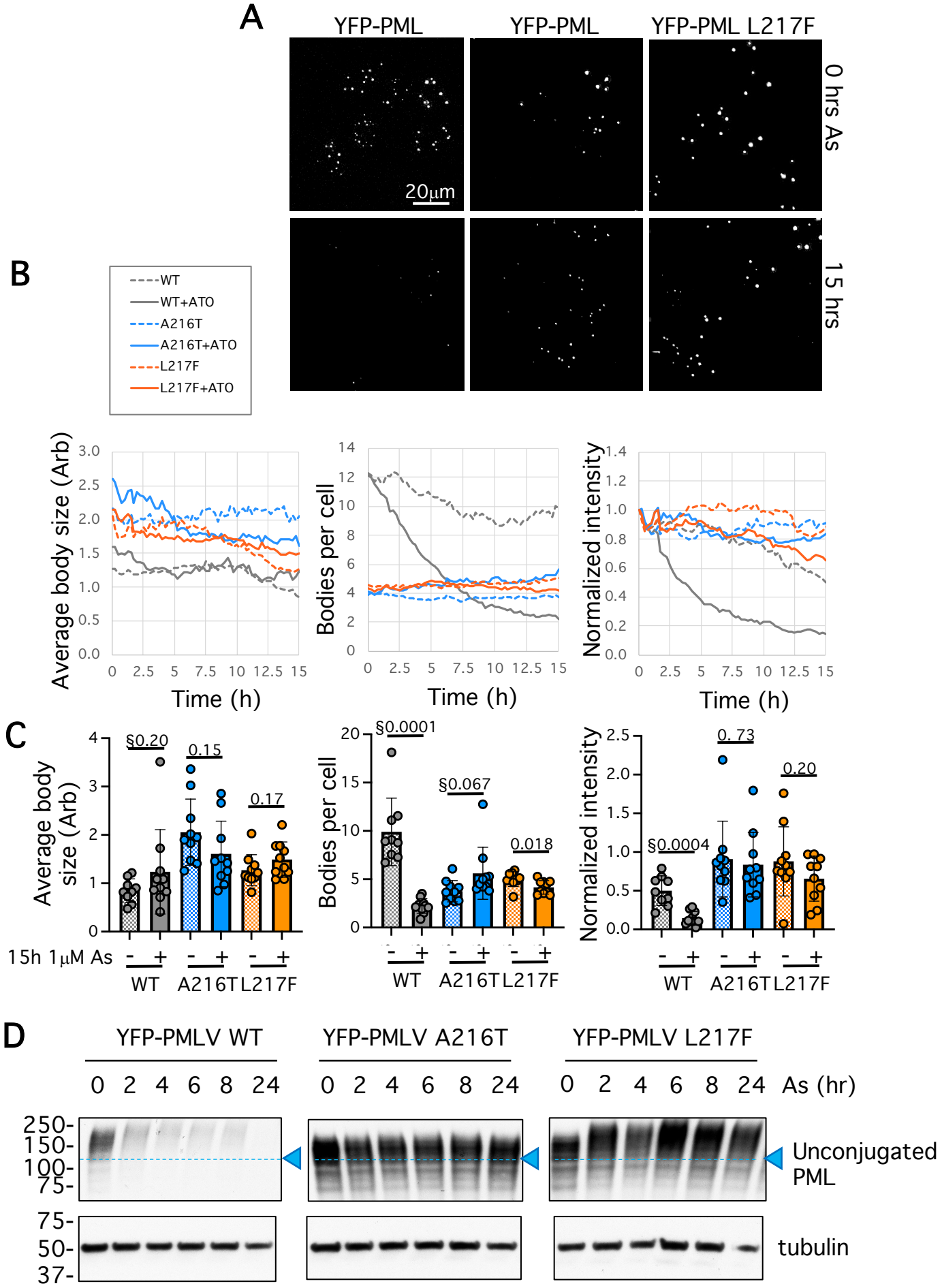

Figure 2. Jaffray et al 2023

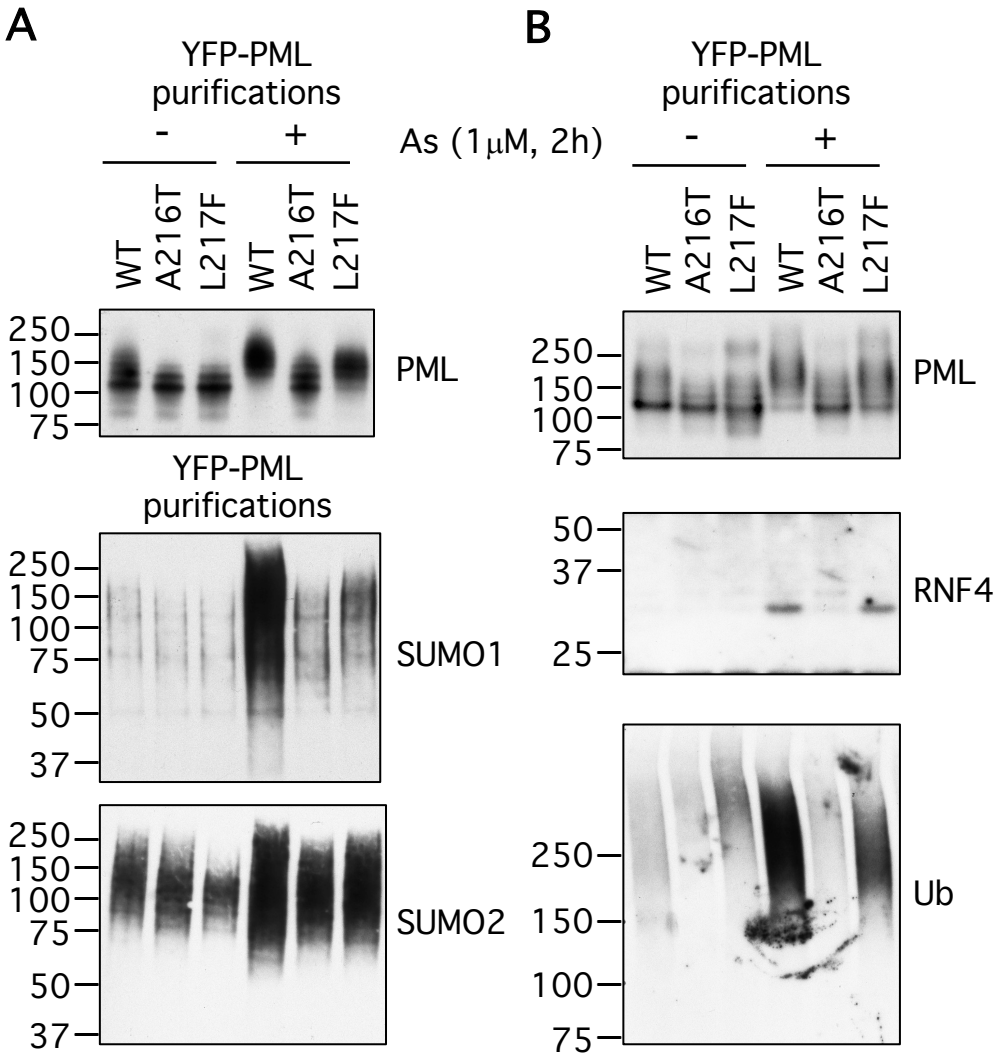

Figure 3. Jaffray et al 2023

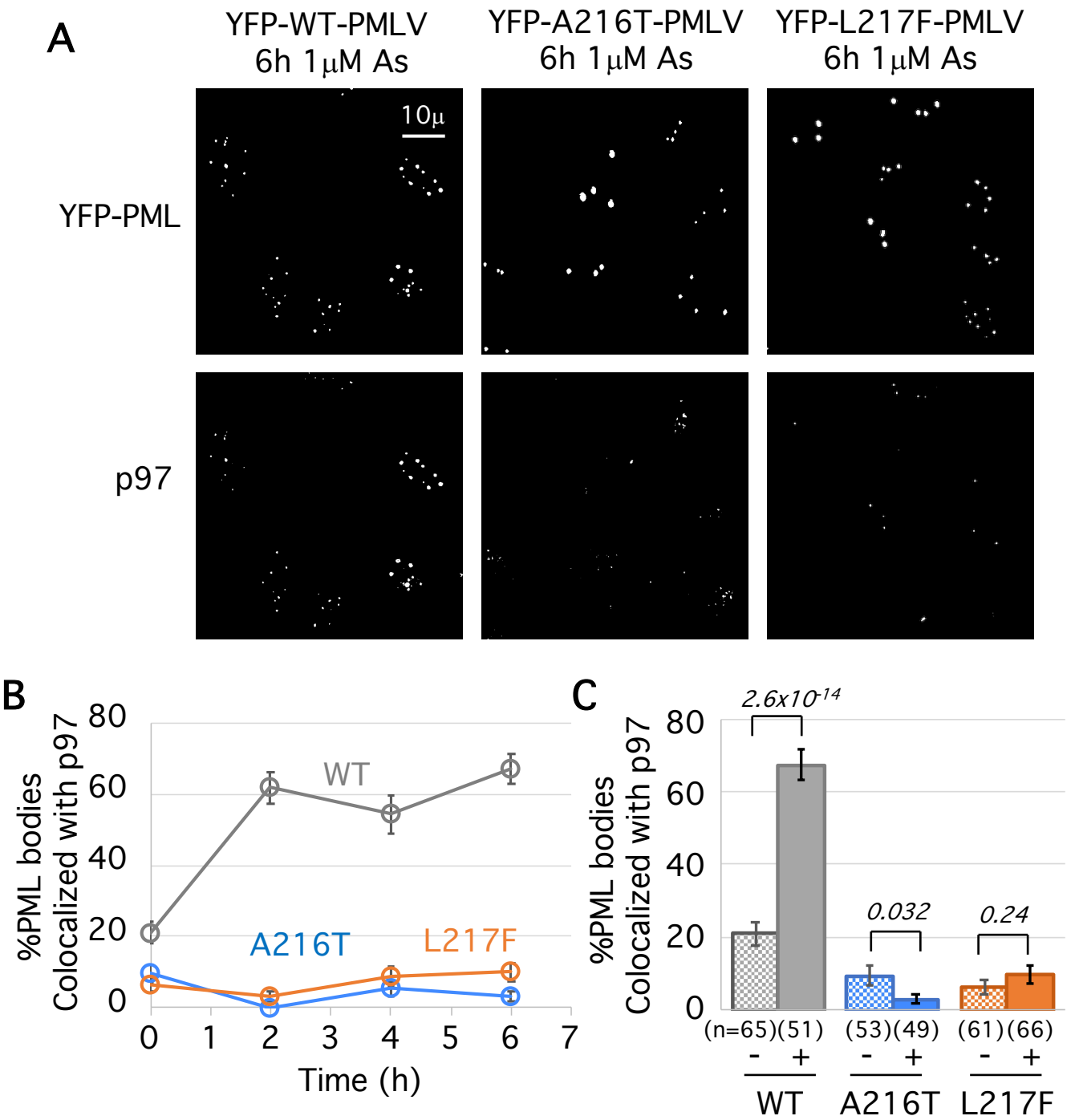

Figure 4. Jaffray et al 2023

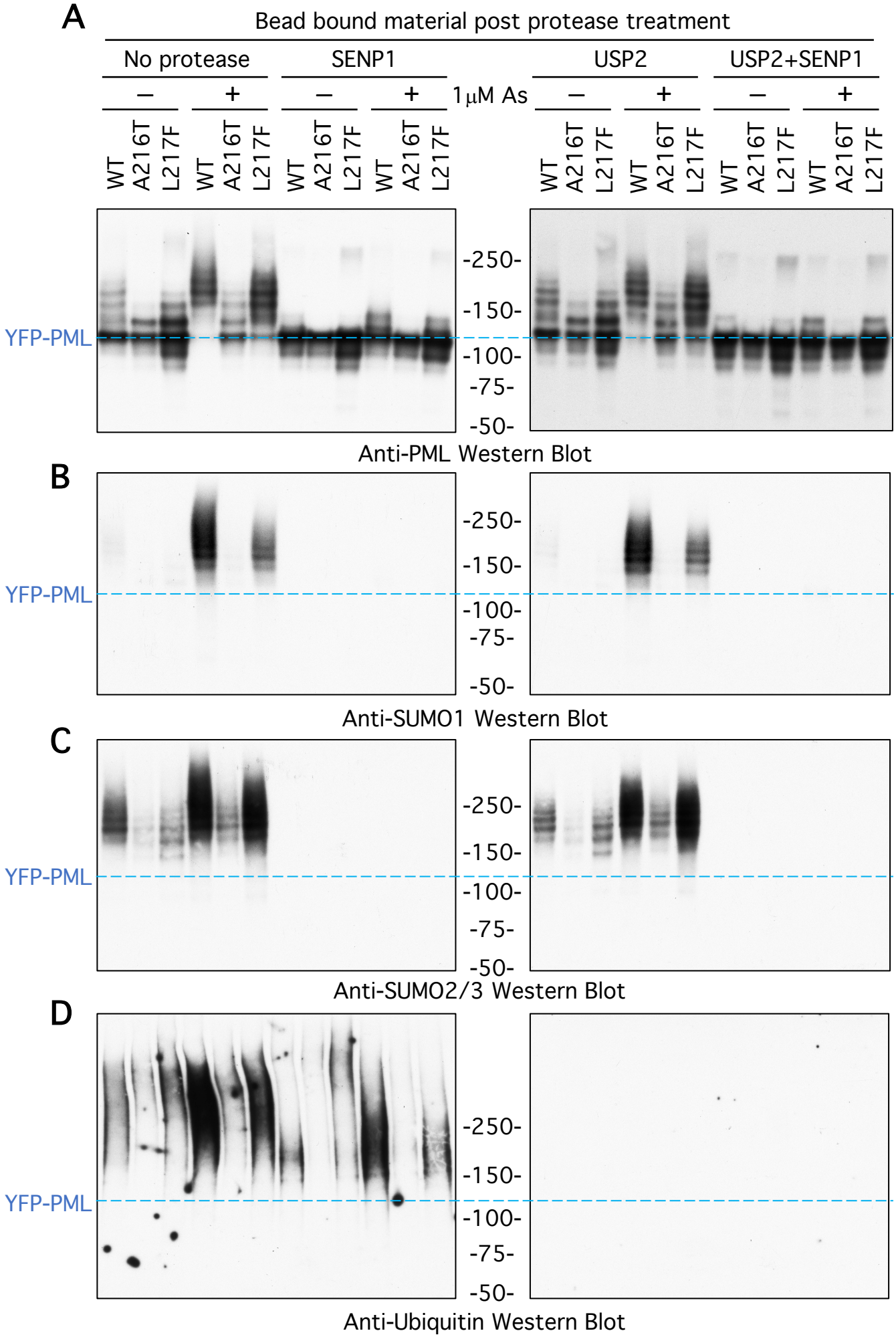

Figure 5. Jaffray et al 2023

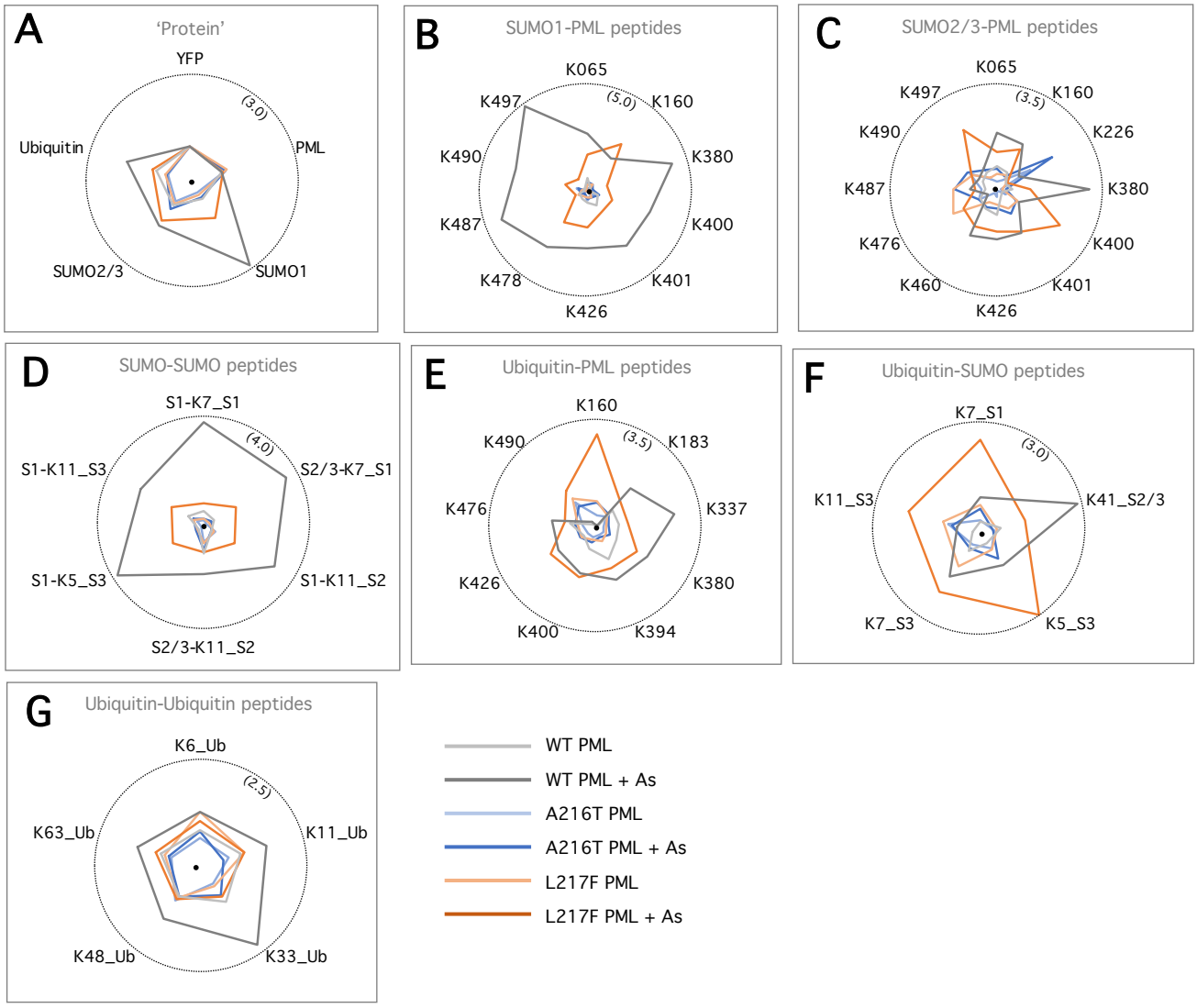

Figure 6. Jaffray et al 2023

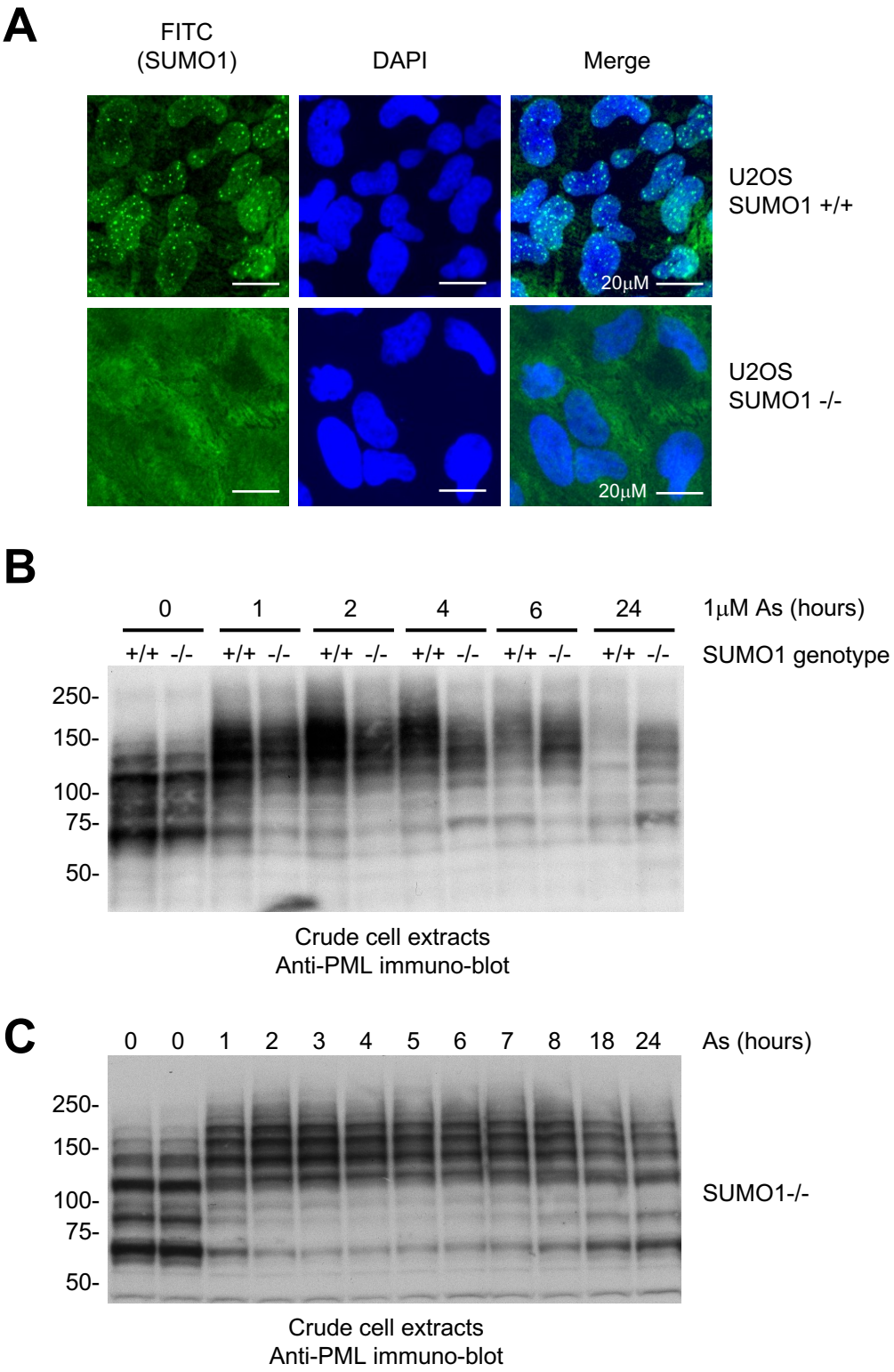

Figure 7. Jaffray et al 2023

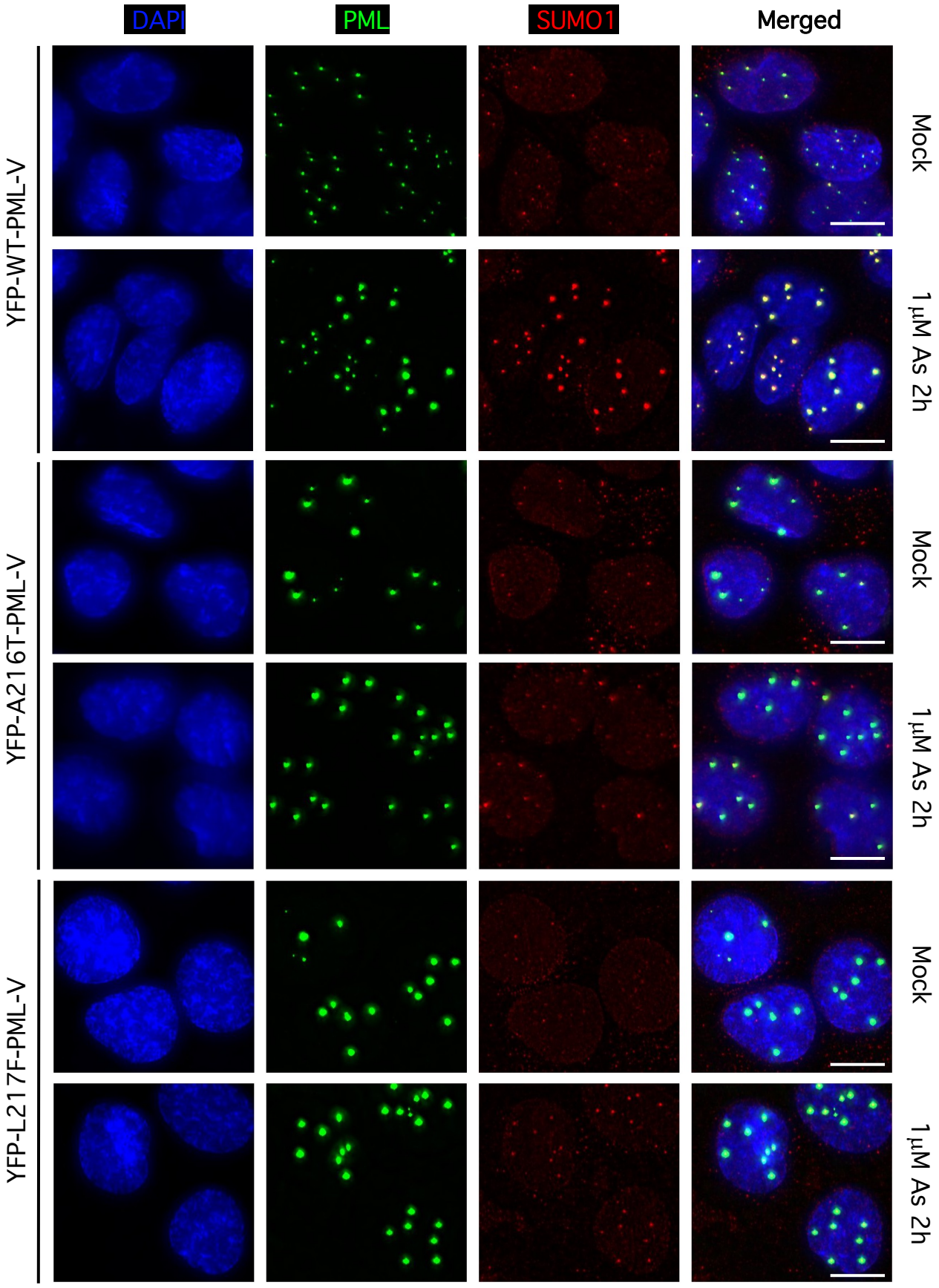

Supplementary Figure 1. Jaffray et al 2023

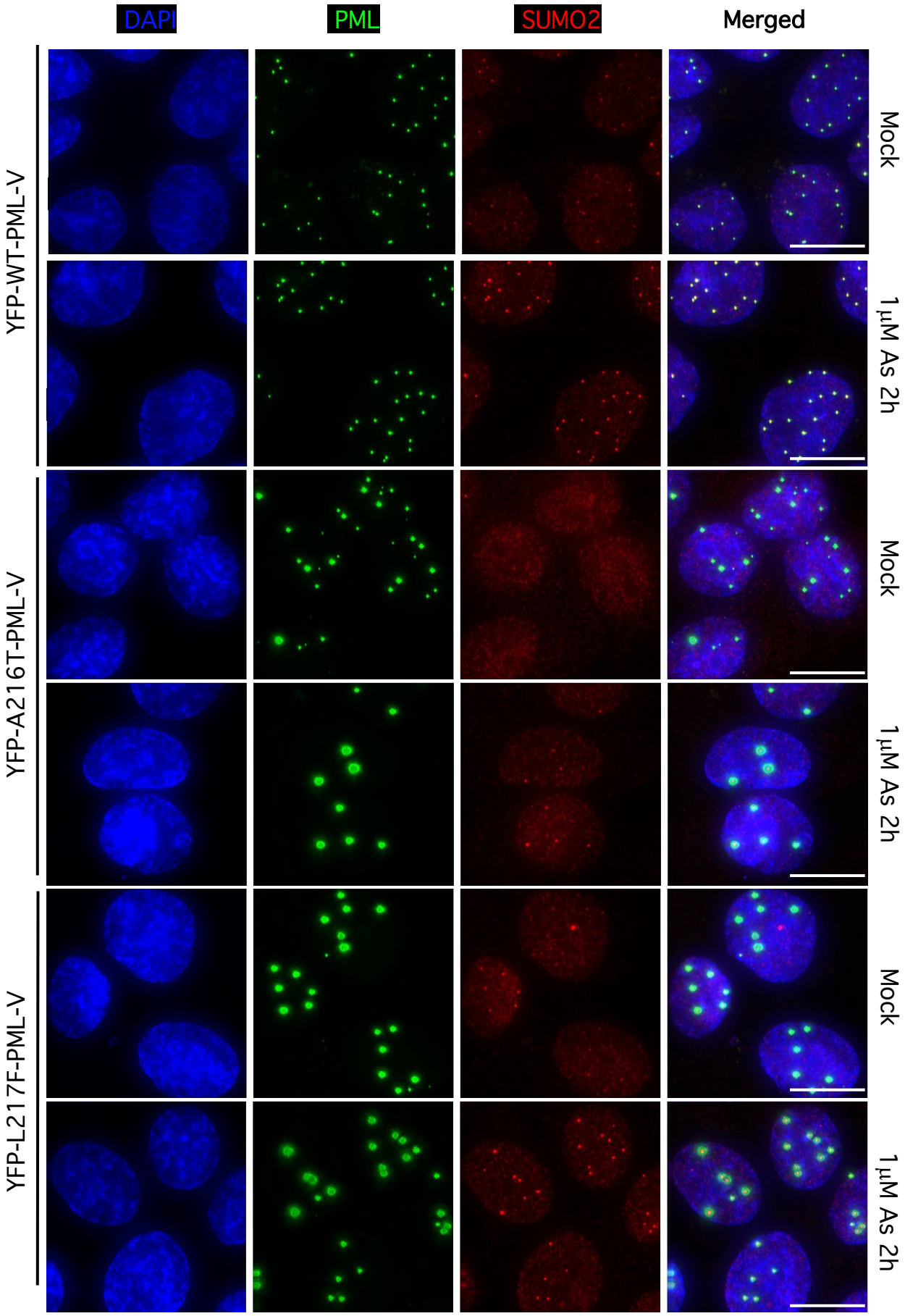

Supplementary Figure 2. Jaffray et al 2023

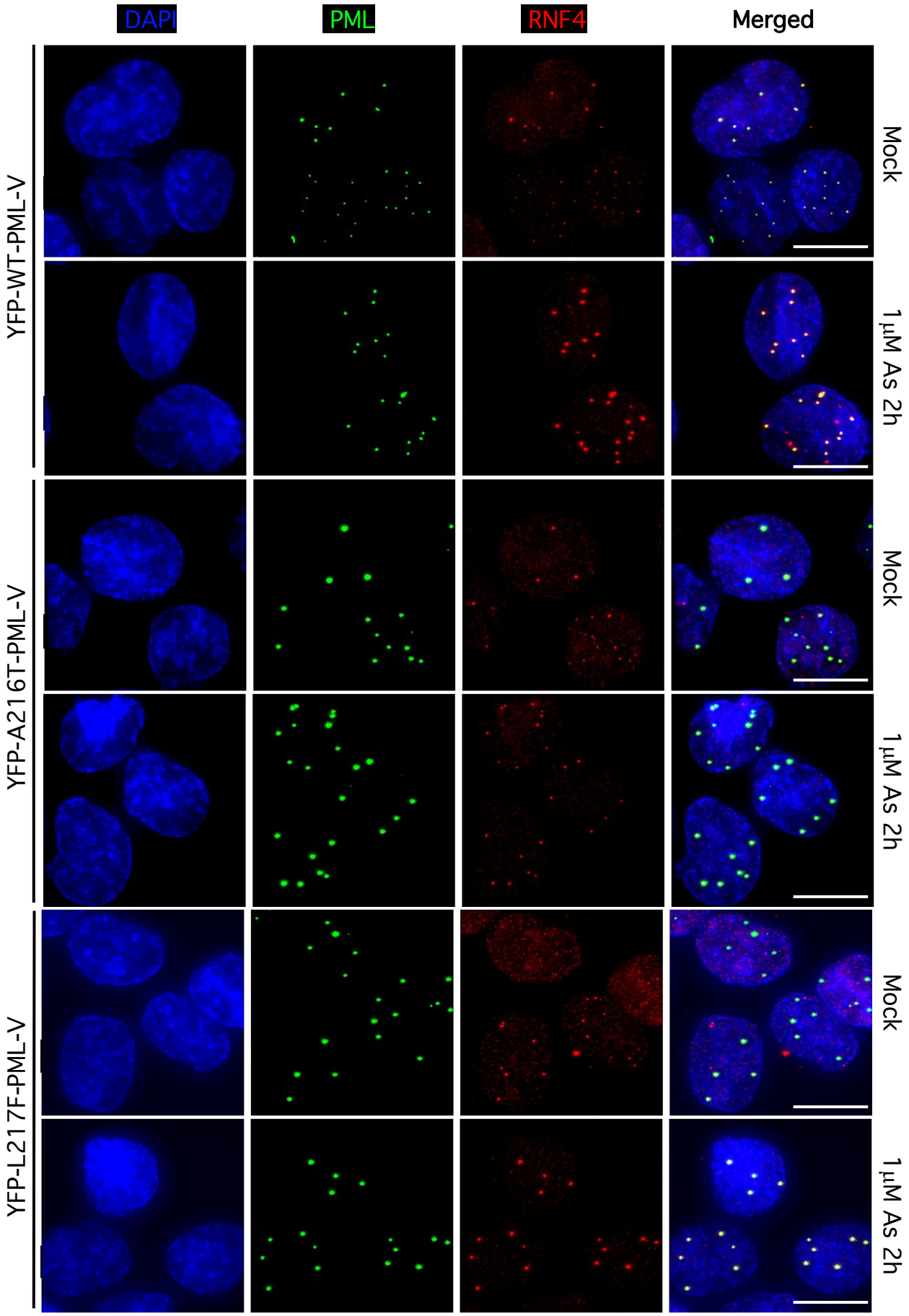

Supplementary Figure 3. Jaffray et al 2023

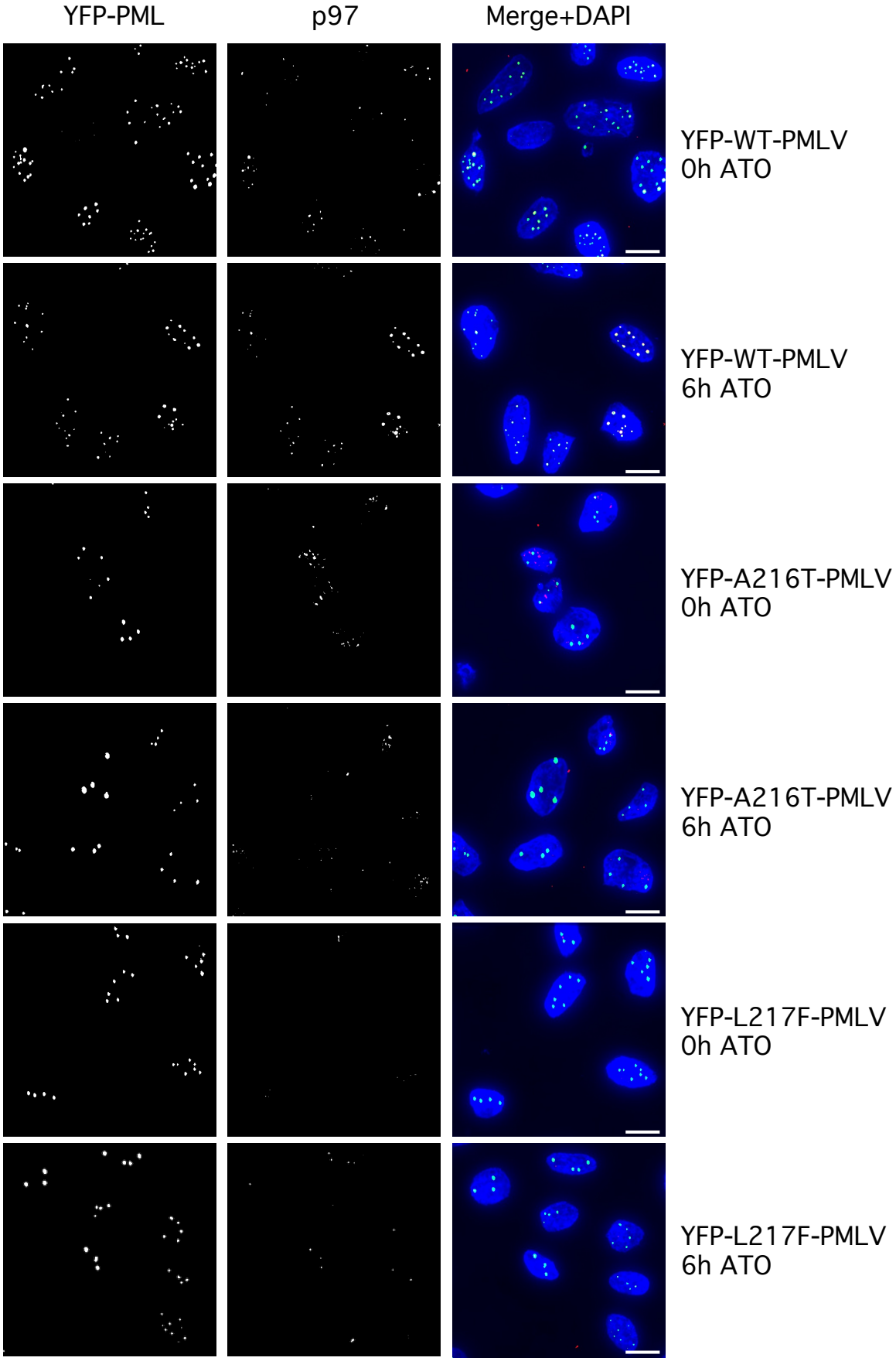

Supplementary Figure 4. Jaffray et al 2023

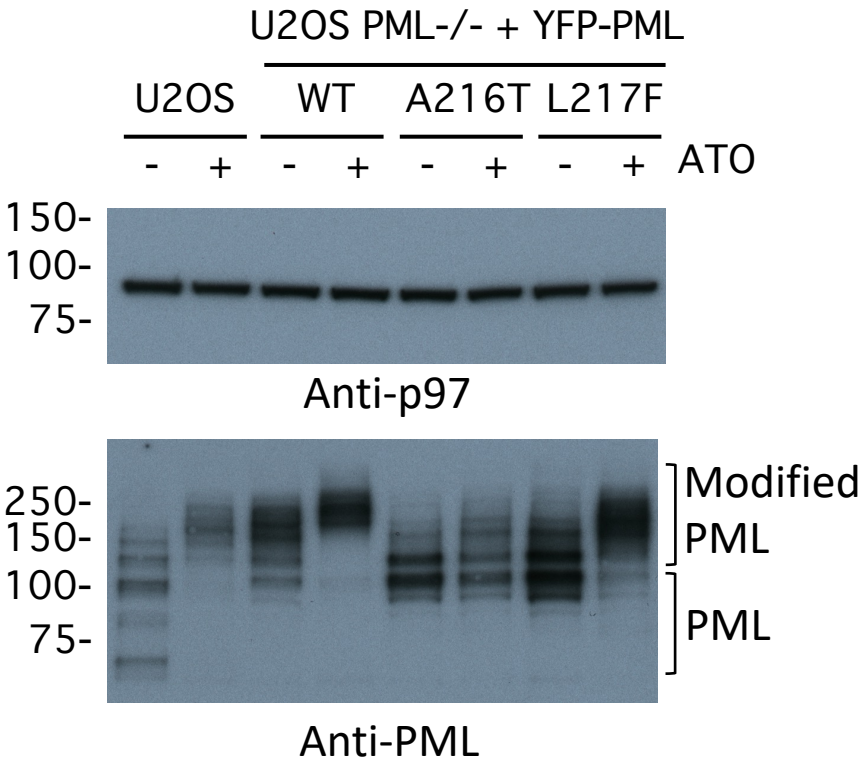

Supplementary Figure 5. Jaffray et al 2023

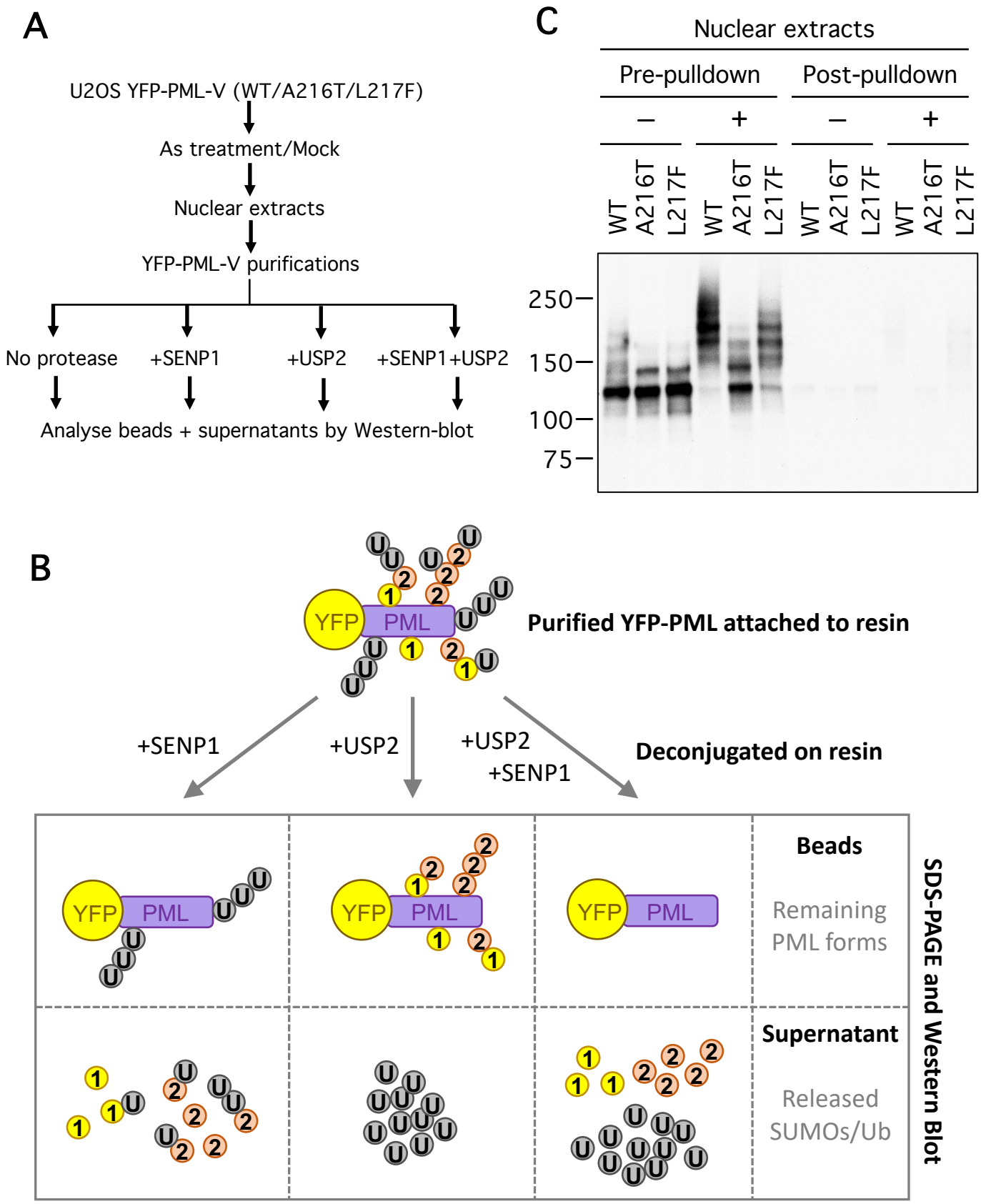

Supplementary Figure 6. Jaffray et al 2023

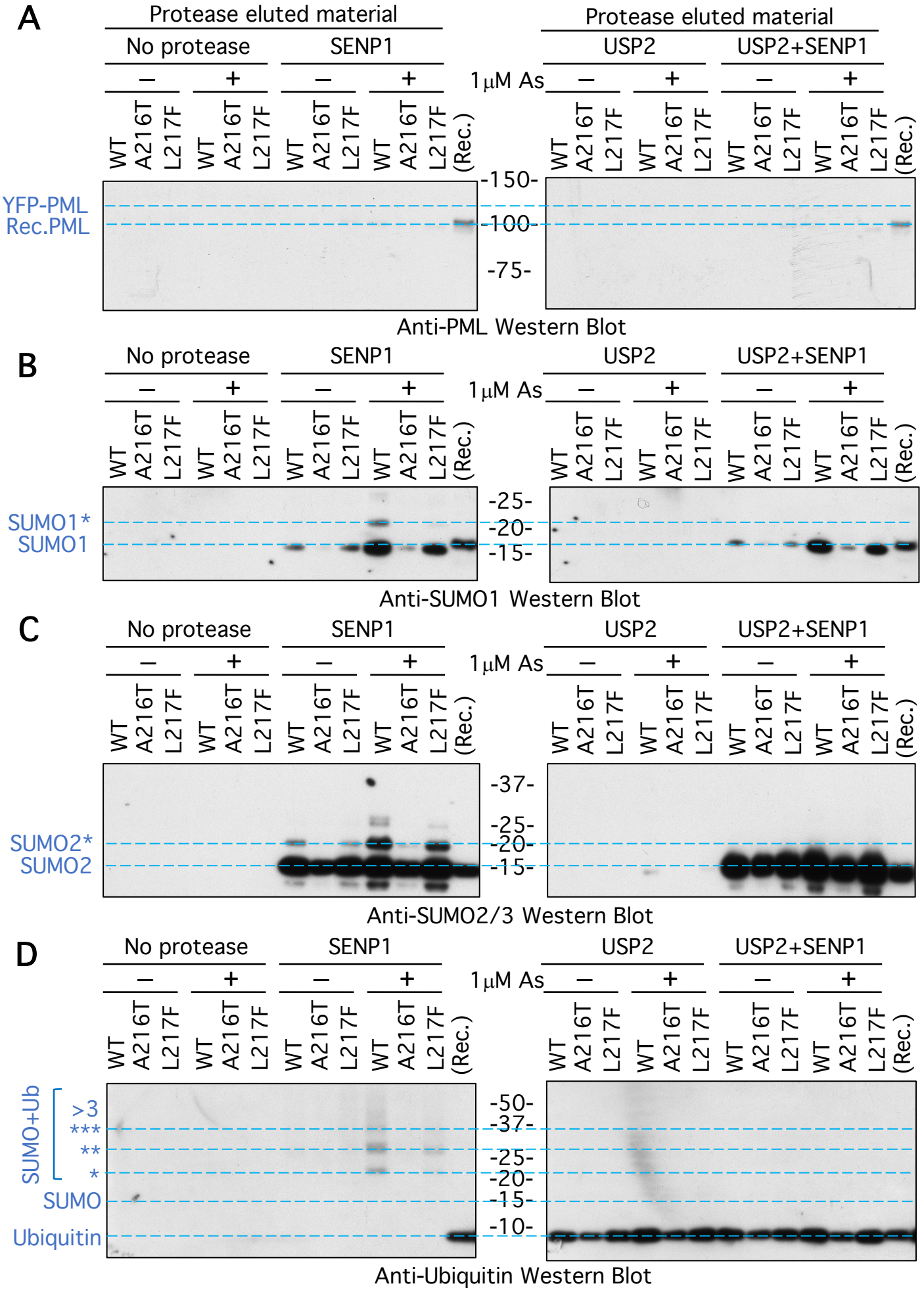

Supplementary Figure 7. Jaffray et al 2023

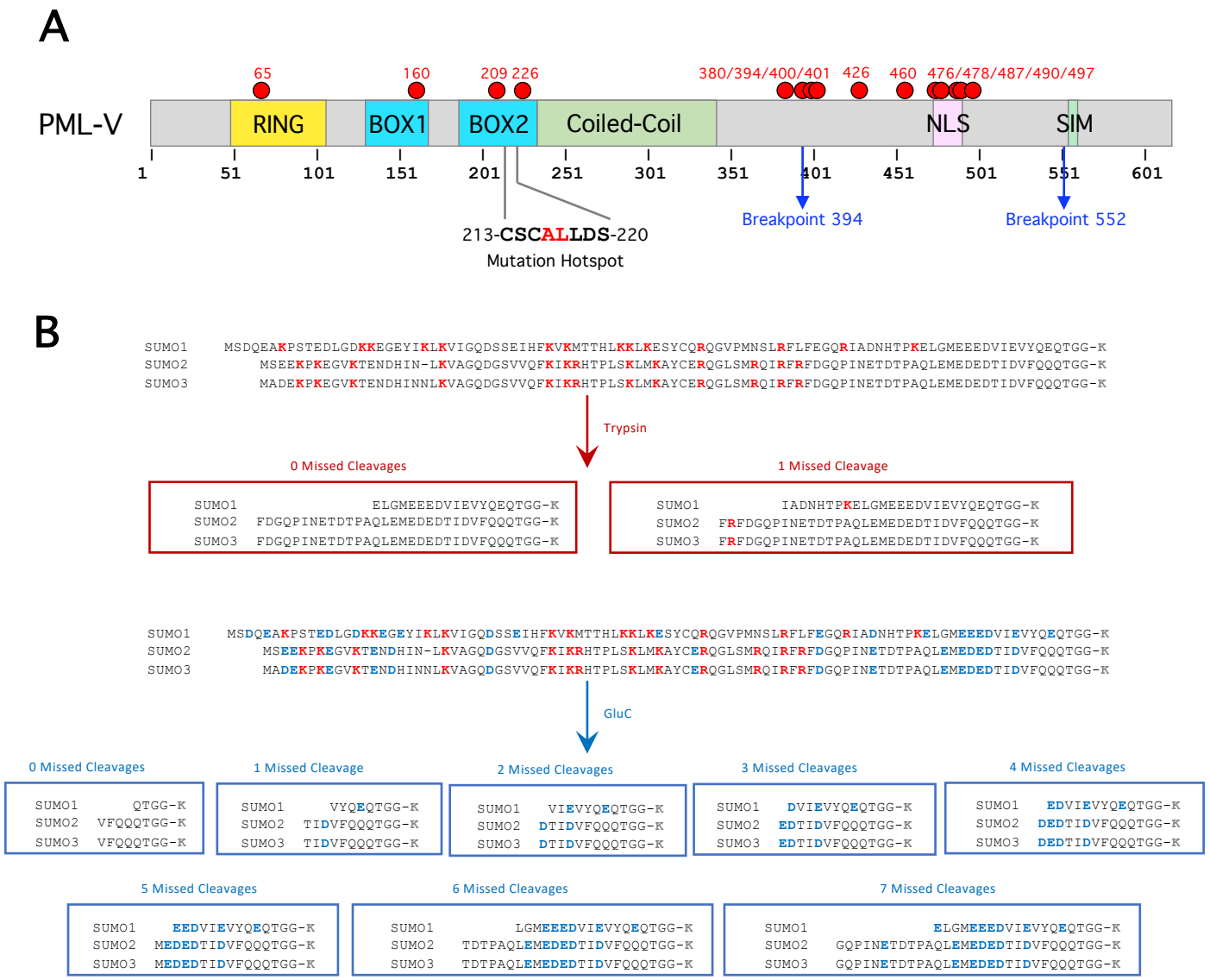

Supplementary Figure 8. Jaffray et al 2023

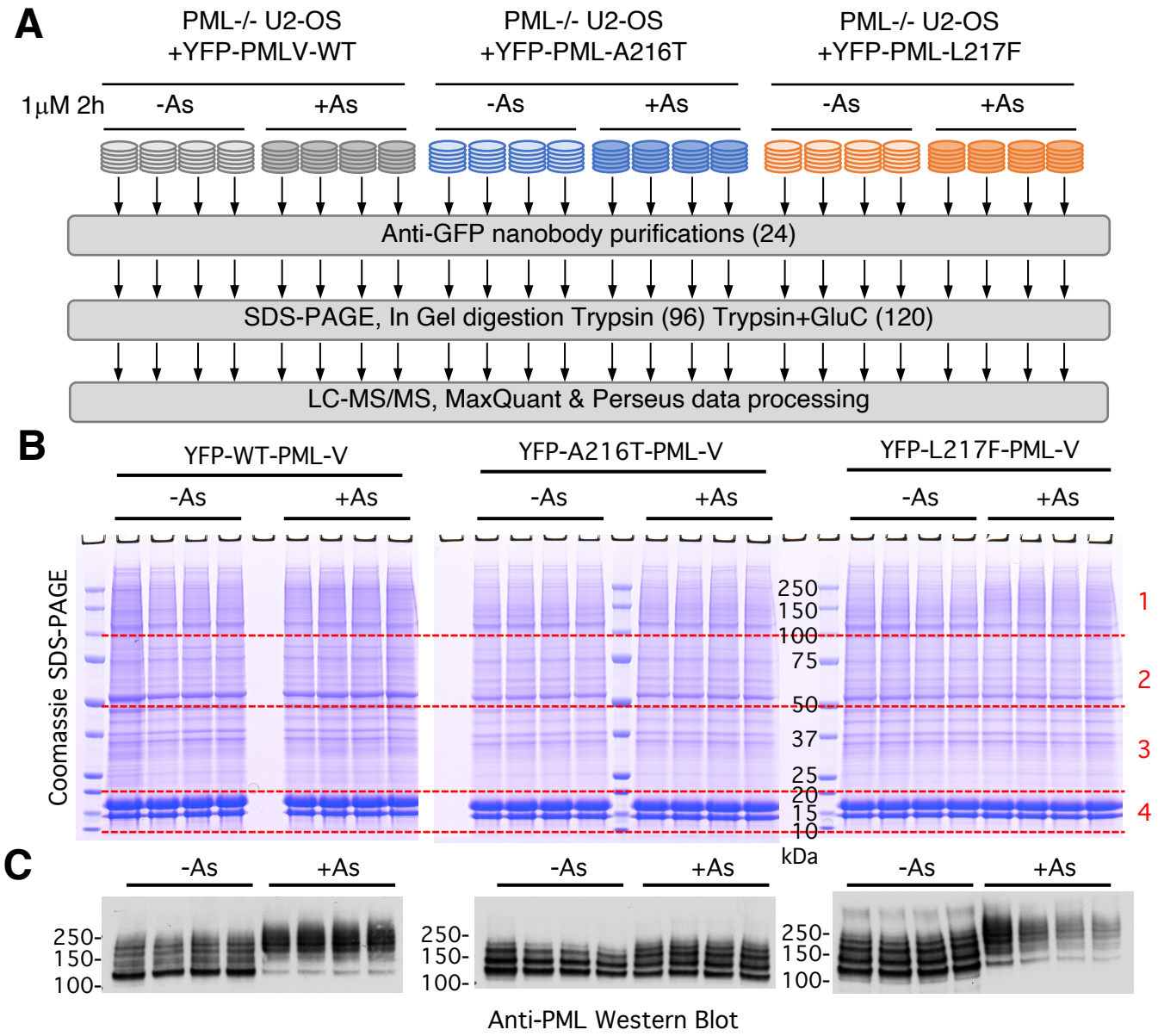

Supplementary Figure 9. Jaffray et al 2023

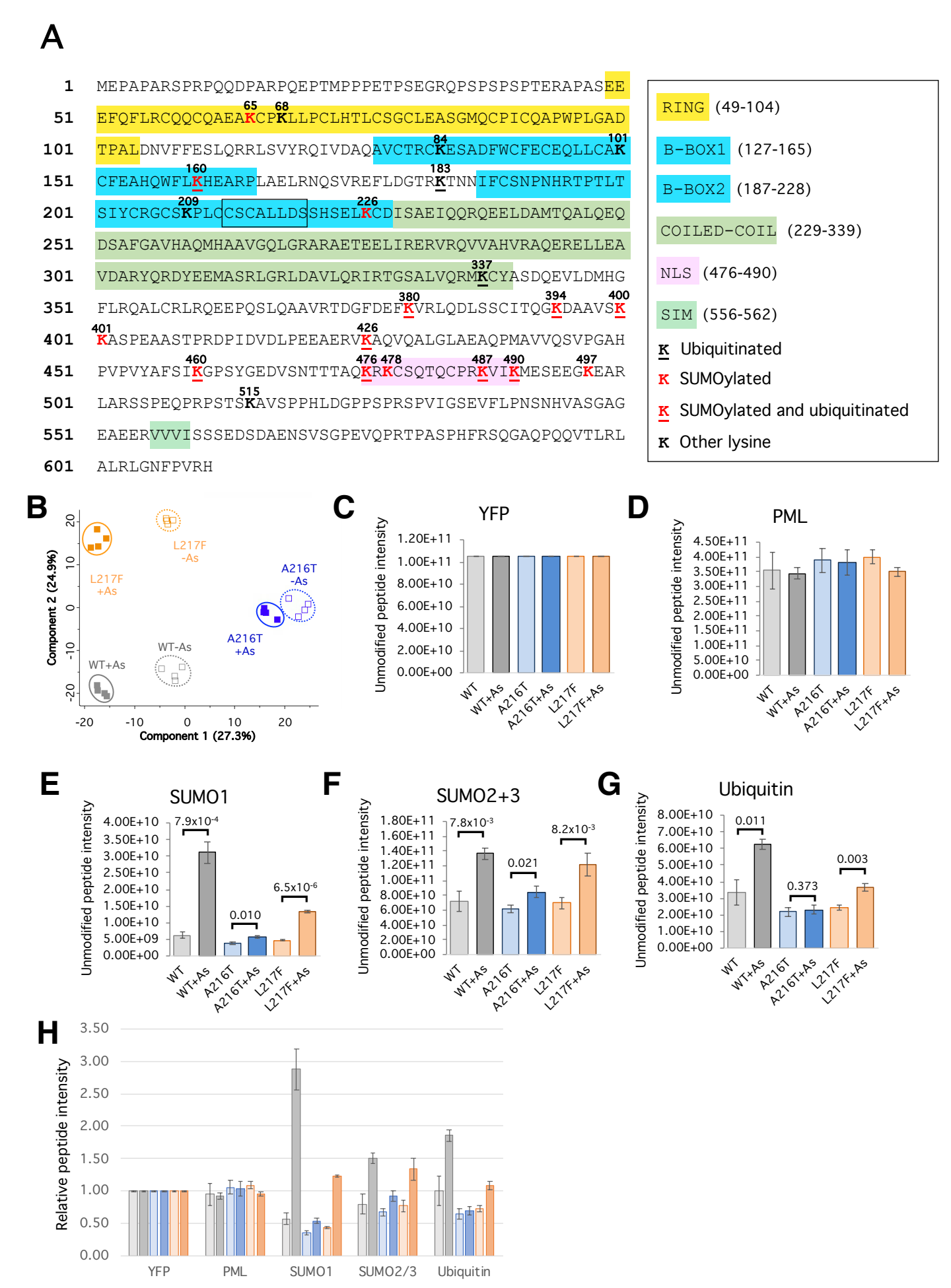

Supplementary Figure 10. Jaffray et al 2023

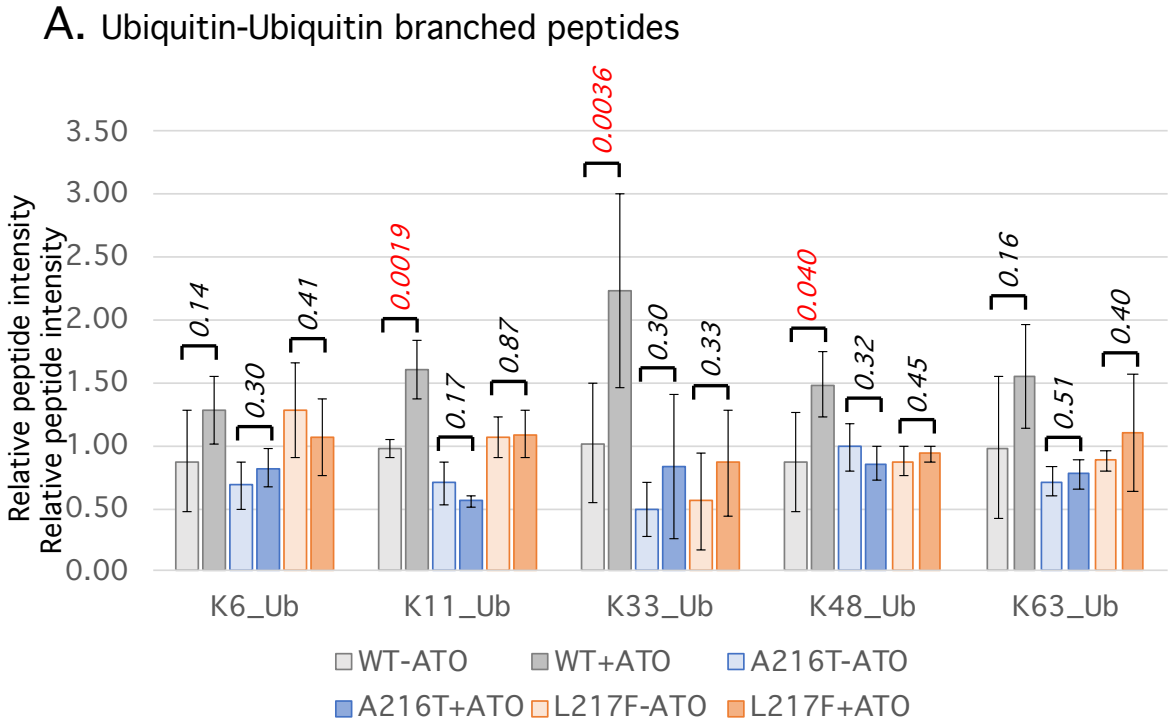

Supplementary Figure 11. Jaffray et al 2023

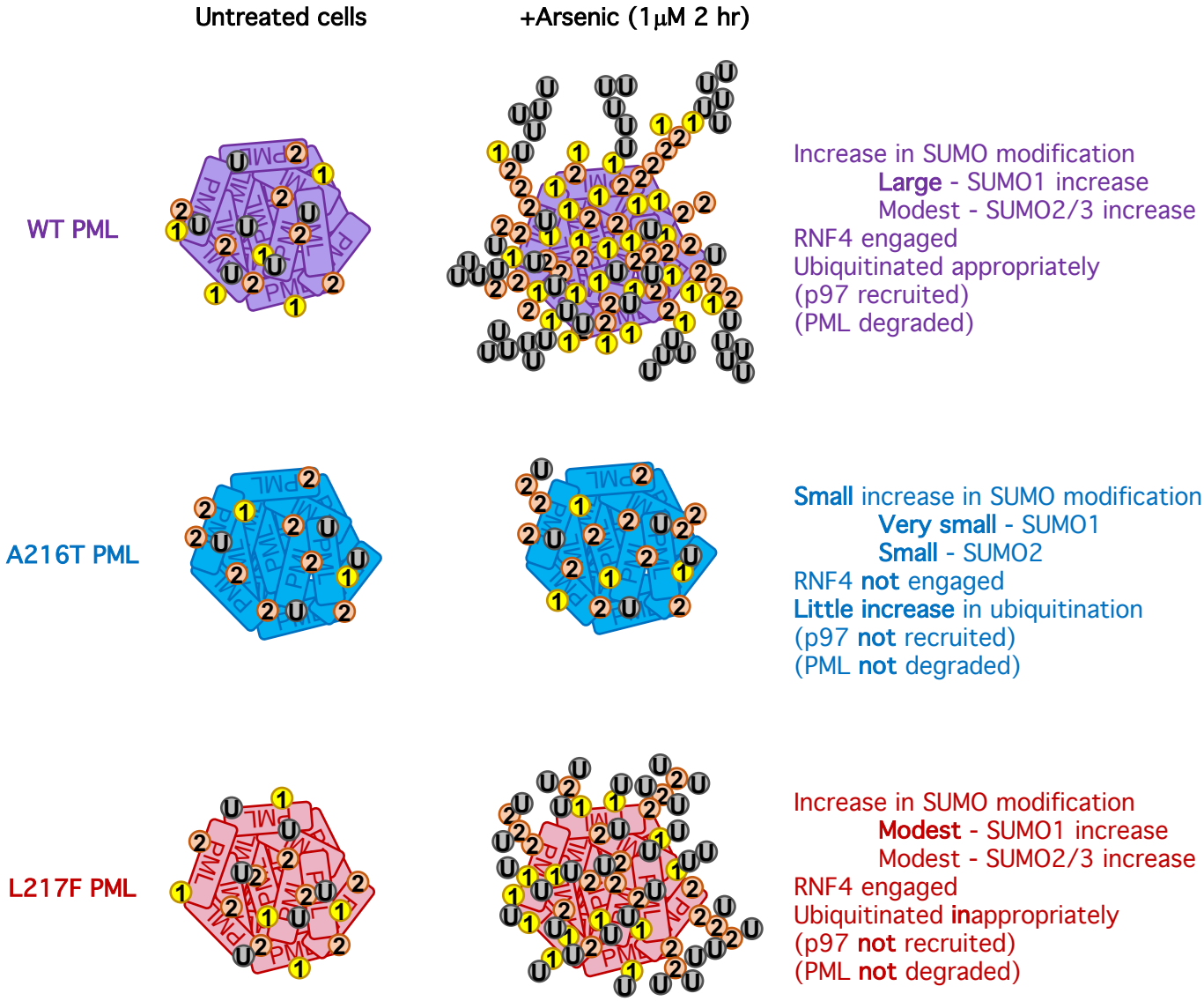

Supplementary Figure 12. Jaffray et al 2023